https://doi.org/10.5194/egusphere-2025-318
Preprint. Discussion started: 24 January 2025

BOSSE v1.0: the Biodiversity Observing System Simulation Experiment

Javier Pacheco-Labrador[1,2], Ulisse Gomarasca[2], Daniel E. Pabon-Moreno[2], Wantong Li[3], Mirco Migliavacca[4], Martin Jung[2], and Gregory Duveiller[2]

[1]Environmental Remote Sensing and Spectroscopy Laboratory (SpecLab), Spanish National Research Council (CSIC), Madrid, 28037, Spain
[2]Max Planck Institute for Biogeochemistry, Jena, D-07745, Germany
[3]Department of Environmental Science Policy and Management, UC Berkeley, Berkeley, CA, USA
[4]European Commission, Joint Research Center, Ispra, Italy

Correspondence to: Javier Pacheco-Labrador (javier.pacheco@csic.es)

Abstract. As global and regional vegetation diversity loss threatens essential ecosystem services under climate change, monitoring biodiversity dynamics and its role in ecosystem services is crucial in predicting future states and providing insights into climate adaptation and mitigation. In this context, remote sensing (RS) offers a unique opportunity to assess long-term and large-scale biodiversity dynamics. However, the development of this capability suffers from the lack of consistent, global, and spatially matched ground diversity measurements that enable testing and validating generalizable methodologies. The Biodiversity Observing System Simulation Experiment (BOSSE) aims to alleviate the lack of this information by means of simulation. BOSSE simulates synthetic landscapes featuring communities of various vegetation species whose traits´s seasonality and ecosystem functions (e.g., biospheric fluxes) respond to meteorology and environmental factors. Simultaneously, BOSSE can generate various types of remote sensing imagery linked to the traits and functions via radiative transfer theory. Specifically, it simulates hyperspectral reflectance factors (R), which can be convolved to the bands of specific RS missions, sun-induced chlorophyll fluorescence (SIF), and land surface temperature (LST). The resolution of the RS imagery can be degraded to test the robustness of different approaches to information loss and the capability of new methodologies to overcome this limitation. Therefore, BOSSE enables users to evaluate the capability of different methods to estimate plant functional diversity (PFD) from RS and link it to ecosystem functions. We expect BOSSE to support the benchmarking and improvement of old and novel methods dedicated to estimating plant diversity and exploring the biodiversity-ecosystem function (BEF) relationships, facilitating advances in this growing area of research and supporting the analysis and interpretation of real-world measurements. We also expect BOSSE to be extended and include new features that provide more realistic simulations that help answer more complex questions related to climate change and global warming.

https://doi.org/10.5194/egusphere-2025-318
Preprint. Discussion started: 24 January 2025

1 Introduction

Climate change and other human-induced environmental changes jeopardize ecosystems' biodiversity and functions, many of which directly translate to ecosystem services (Hernández-Blanco et al., 2022). Biodiversity can sustain the stability of ecosystem functions, such as photosynthesis or transpiration, in response to environmental variability, perturbations, and extreme events (Mahecha et al., 2023; De Bello et al., 2021). Many terrestrial ecosystem functions and services depend on plant diversity, as plants are the primary producers in terrestrial ecosystems, i.e., they produce the chemical components that support other living beings (Isbell et al., 2011). Therefore, it is necessary to establish a system for global plant diversity monitoring to assess and quantify biodiversity loss, sustain ecosystem stability, and forecast future scenarios (Gonzalez et al., 2023; Pereira et al., 2013). In this context, remote sensing (RS) has become a valuable tool, given its capability to provide continuous and synoptic information on the Earth's surfaces (Cavender-Bares et al., 2017). Since the proposition of the Spectral Variation Hypothesis (SVH) (Palmer et al., 2000), the spatial variability of spectral signals and RS products has been related to different facets of vegetation diversity, such as taxonomic (Van Cleemput et al., 2023), functional (Ma et al., 2019), and phylogenetic (Schweiger et al., 2018) diversity; moreover, recent works have also linked RS-derived diversity with ecosystem functional properties (Gomarasca et al., 2024). However, other studies have also reported RS failing to capture different facets of plant diversity, at least in particular cases (Ludwig et al., 2024; Fassnacht et al., 2022; Van Cleemput et al., 2023).

The evaluation of the SVH is challenging since the test outcome strongly depends on the data used (e.g., field sampling schemes, sensor features, and resolutions), the methodologies and metrics quantifying diversity, and the type and extent of the study sites. The variability and lack of overlap of these factors lead to a broad spectrum of results (Torresani et al., 2024), which are not systematically comparable. Since most studies are limited in all these aspects, it remains unclear whether the hypothesis should be discarded or whether the methods and data fail to capture plant diversity. The underlying problem is a lack of consistent global databases (meaning representative of the Earth´s terrestrial ecosystems) to develop, compare, and identify reliable methodologies. Furthermore, the relationships established between RS and field estimates of plant diversity are often indirect due to a lack of physical connection between the variables measured in the field and the spectral signals of vegetation. This lack of connection limits the interpretation and generalization of the results and might make the estimation of some diversity facets unreliable and context-dependent (e.g., taxonomic diversity (Fassnacht et al., 2022)). Among all the diversity facets, plant functional diversity (PFD) is the most directly (physically) linked to RS data since it relies on the physical properties of vegetation that determine its interaction with radiation. However, not all traits or their measurements feature this physical link. For example, ecological surveys often measure plant traits on a per-leaf mass basis, which are less connected to the spectral signals captured by RS than if measured per-leaf area (Kattenborn et al., 2019). In addition, the effect of the measurement uncertainties and spatial mismatches between field and RS data is poorly understood and could induce spurious relationships and conclusions (Pacheco-Labrador et al., 2022). Consequently, despite multiple studies (for a

https://doi.org/10.5194/egusphere-2025-318
Preprint. Discussion started: 24 January 2025

literature review, see Torresani et al.(2024)), basic methodological questions remain unanswered, and there is a risk that methodologies prone to spuriousness are identified as adequate and others more suitable pass unnoticed.

Generating consistent datasets for robust methodological benchmarking and SVH evaluation would require great coordination efforts and dedicated field sampling protocols rarely used by ecologists or remote sensing scientists. On the one hand, the plant traits targeted by ecologists (characteristics of organisms that influence performance or fitness), along with their sampling schemes, are not optimized for evaluating RS-based estimates of biophysical variables or their diversity. On the other hand, adapting the typical sampling schemes in RS to facilitate the evaluation of diversity estimates could require both *n*-folding the sampling effort (e.g., multiplying the number of sampling plots to build *n*-by-*n* grids as in Hauser (2021)) and making sure that the variables (traits) that significantly influence the spectral signals are effectively measured. Furthermore, optimized samplings should be applied in research stations where ecosystem functions are also measured so that methods to assess BEF relationships using remote sensing -a nascent research field- can be robustly developed. Nowadays, even the most promising coordinated activities in this direction (Barnett et al., 2019) lack sampling protocols fully optimized for testing the SVH and benchmarking RS methods, despite which these efforts are extremely valuable.

Alternatively, some researchers have used radiative transfer models to overcome the lack of suitable field datasets (simulating them instead) and answer methodological questions regarding the capability of RS to infer different plant taxonomic (Badourdine et al., 2023; Fassnacht et al., 2022; Van Leeuwen et al., 2021) and functional diversity (Pacheco-Labrador et al., 2022; Ludwig et al., 2024). Simulations have also helped to understand the results found using RS data to assess BEF relationships (Gomarasca et al., 2024). Within the limitations of the synthetic data, these works have provided valuable insights into methodological questions and framed the chances of RS to infer plant diversity within wide ranges of situations that exceed those covered by local and individual studies. Radiative transfer simulations have also helped to test new diversity metrics optimized for RS data (Pacheco-Labrador et al., 2023). However, these works have been relatively limited regarding the simulation of multiple spectral signals, the incorporation of phenology, the spatial representation of landscapes, the corresponding RS imagery, and the connection of spectral signals with ecosystem functions.

This manuscript presents the Biodiversity Observing System Simulation Experiment (BOSSE), a modeling tool to advance the development of RS methods to monitor PFD and BEF relationships from space. BOSSE simulates 1) spatially explicit scenes (vegetation-populated landscapes) where plant traits (PT) and the associated functions (e.g., biospheric fluxes) respond to meteorology and environmental factors, and 2) the physically and physiologically connected imagery of hyperspectral reflectance factors (*R*), sun-induced chlorophyll fluorescence radiance (*F*), land surface temperature (LST), and retrieved optical traits (OT). BOSSE v1.0 is designed to benchmark metrics and methods that cope with the challenges of using RS data to capture PFD and relate the PFD estimates with ecosystem functions in space and time, allowing for a flexible configuration of the simulations, e.g., degrading sensor resolutions while always providing a reference or best-case scenario. We expect BOSSE to help the RS community benchmark and develop their methods in a controlled environment, supporting the interpretation and design of experiments and measurements.

https://doi.org/10.5194/egusphere-2025-318
Preprint. Discussion started: 24 January 2025

2 Methods

2.1 BOSSE model

The BOSSE model v1.0 is a spatially defined dynamic vegetation model able to simulate maps of plant traits, functions (e.g., biospheric fluxes), and the physically and physiologically connected remote sensing imagery in the optical domain at hourly steps. It allows various configuration options that enable repeatable simulations featuring different spatial patterns, climatic and meteorological conditions, taxonomic richness, spatial and temporal resolutions, or simulated satellite missions. A BOSSE "Scene" is a configurable synthetic landscape containing species' individuals whose properties and functions evolve in response to meteorology and other spatially varying environmental conditions (e.g., soil properties). BOSSE conceives a plant "species" as a classification rather than an evolutionary unit (Dupré, 2001). A species is defined as a unique set of variables (phenological maximum and minimum radiative transfer variables and phenological model parameters, among others) that is randomly generated. Moreover, BOSSE simulates intra-specific variability so that each species represents the averaged specific phenotype and response to the environment (phenology) of a group of individuals. Consequently, in the simulated plant traits maps, each pixel shows unique values that differ to some degree from the values of the pixels corresponding to the same species. This variability propagates to the spectral signals and functions related to each pixel. Despite operating on a continuous trait space, each species is associated with a given plant functional type (PFT), which constrains the range of variability and sometimes the covariance between traits and the relative abundance as a function of the simulated Köppen climatic zone.

Fig. 1 summarizes BOSSE's workflow, which is divided into three phases (the last one, "Analyses", is to be implemented by the user). BOSSE is coded in Python 3.11 as a Class to facilitate usability. The source code and a Jupyter tutorial are published on GitHub (https://github.com/JavierPachecoLabrador/pyBOSSE) under the GPL-3 license.

- Initialization of the BOSSE class. Each simulation location is assigned to a given climatic zone that determines the presence and the probability of occurrence of the different PFTs represented (Supplementary Material S1). Moreover, meteorological data time series (e.g., radiation, air temperature, soil moisture) are used with a phenological model to filter out the least competitive PFTs under those conditions. Then, one or more species are assigned to each PFT. The individuals of the different species are located in space, assuming each pixel is occupied by one individual or a group of identical individuals and, therefore, it contains a unique set of plant trait values. Then, the maximum and minimum values of all traits (i.e., radiative transfer variables) are defined for each pixel.
- Simulation: Once BOSSE is initialized for a given Scene, the phenological model parameters and the trait ranges determine the trait values of each individual at any given time as a function of meteorology. The results of this step are plant trait maps and the corresponding RS imagery and ecosystem functions.
- Analyses: The user can use BOSSE outputs to compute functional diversity metrics from the simulated trait maps and the simulated RS imagery. It is also possible to derive ecosystem functional properties from the ecosystem functions. These products can be used to benchmark different methods and answer methodological questions (e.g.,

https://doi.org/10.5194/egusphere-2025-318
Preprint. Discussion started: 24 January 2025

which variables capture the best plant diversity or BEF relationships). In this manuscript, we exemplify the analysis of BOSSE v1.0 outputs with the Python package "pyGNDiv" (https://github.com/JavierPachecoLabrador/pyGNDiv-master) (Pacheco-Labrador et al., 2023) recently updated with "numba" (Lam et al., 2015) compilation for faster computation and new features to directly asses cubes of RS imagery, products or plant trait maps. pyGNDiv provides a selection of benchmarked functional diversity metrics and methods for partitioning diversity at different scales (Pacheco-Labrador et al., 2023; Pacheco-Labrador et al., 2022) such as Rao's quadratic entropy index Q_{Rao} (Botta-Dukát, 2005)) and the fractions of α (f_α) and β-diversity (f_β) using a variance-based approach (Laliberté et al., 2020)). In addition, pyGNDiv normalizes the value of the metrics by the number of variables so that these are comparable one-to-one, independently of the number of traits or spectral bands analyzed. At this stage, the users can also test and benchmark their own methods and metrics.

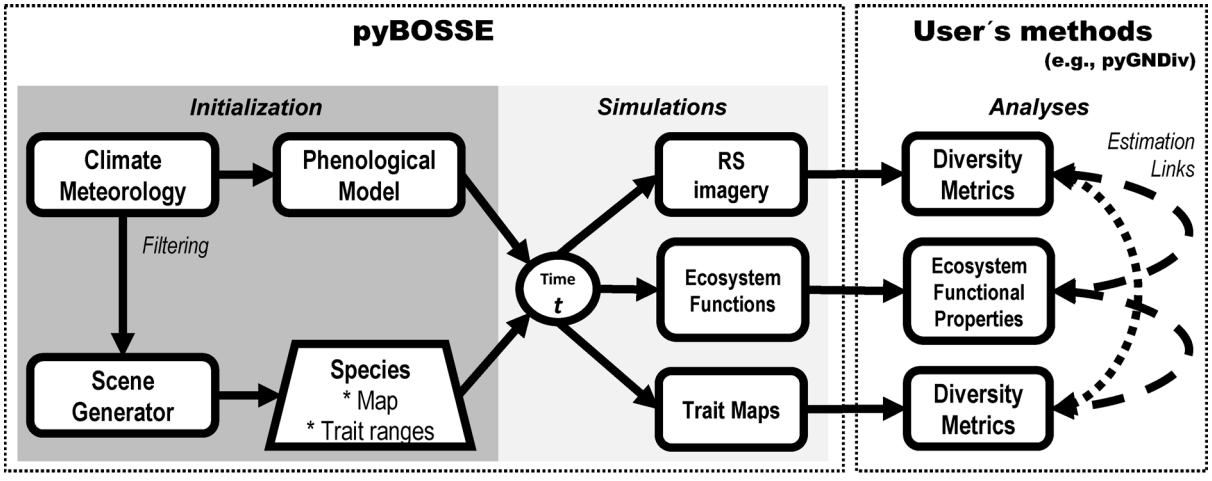

Figure 1: Biodiversity Observing System Simulation Experiment (BOSSE) workflow.

2.2 BOSSE data and data-driven submodels

BOSSE combines data and several models parametrized from different datasets or bibliographic references.

2.2.1. Plant functional types and climatic zones

We determined the relative abundance of different PFTs in each Köppen climatic zone by convolving the European Space Agency's Land Cover Climate Change Initiative (ESA LC-CCI) Global Plant Functional Types Dataset (v.2.08) from Harper et al. (2023) with the Köppen Climate Classification System maps from Rubel et al. (2017). We also considered the estimates of C3/C4 grass leaf area fraction generated in the NACP MsTMIP simulations (Global 0.5-degree Model Outputs

https://doi.org/10.5194/egusphere-2025-318
Preprint. Discussion started: 24 January 2025

in Standard Format, Version 2.0, from Huntzinger et al. (2021)) to separate the Grasses PFTs (Supplementary Material 1). These probabilities are used to determine the number of species belonging to a PFT when a Scene is generated.

2.2.2 Meteorological data

For each climatic zone, we selected 15 random locations (60 sites total) where we downloaded two years (2020-2022) of ERA5-Land hourly meteorological data (Supplementary Material S2). Accumulated radiation was recomputed to instantaneous rates ([W m-2]) and accumulated precipitation at hourly intervals. The selected variables were prepared as the inputs of the model SCOPE (Van Der Tol et al., 2009) as in Li et al. (2023) (Table S2.1).

2.2.3 Plant traits and random generator

BOSSE randomly generates sets of plant traits (i.e., radiative transfer model variables) for each pixel of a Scene, each representing a species individual or group of identical individuals. This can be constrained by PFT-dependent bounds or consider empirical relationships between traits (Table 1). BOSSE preserves the covariance between most foliar traits by drawing them from a Gaussian Mixture Model (GMM) trained over a 16703 samples database generated by combining and gap-filling different spectral libraries and the TRY database (Kattge et al., 2020) (Supplementary Material S3). The maximum carboxylation at optimal temperature (V_{cmo}) rate is then predicted as a PFT-dependent function of chlorophyll content (C_{ab}). Most structural parameters are sampled from uniform distributions within global or PFT-dependent bounds. Canopy height (h_c) is derived as a function of leaf area index (LAI).

Table 1. BOSSE plant traits and variables, symbols, bounds, and the method used to produce them in the simulations

Plant trait	Symbol	Units	Bounds	Simulation
Leaf structural parameter	N	layers	[1, 3.6]	Random, GMM
Leaf chlorophyll content	C_{ab}	µg cm^{-2}	[0, 100]	Random, GMM, with PFT-dependent bounds from Croft (2017)
Leaf carotenoids content	C_{ca}	µg cm^{-2}	[0, 40]	Random, GMM
Leaf anthocyanins content	C_{ant}	µg cm^{-2}	[0, 10]	Random, GMM
Leaf senescent pigments content	C_s	a.u.	[0, 3]	Random, GMM
Leaf water content	C_w	g cm^{-2}	[0.004, 0.081]	Random, GMM
Leaf dry matter content	C_{dm}	g cm^{-2}	[0.019, 0.030]	Random, GMM
Leaf inclination distribution function	$LIDF_a$	-	[-1, 1]; $\|LIDF_a + LIDF_b\| \leq 1$	Random, uniform distribution with global bounds
Bimodality of the leaf inclination	$LIDF_b$	-		
Leaf area index	LAI	m^2 m^{-2}	[0, 15]	Random, uniform distribution with PFT-dependent bounds from Asner

https://doi.org/10.5194/egusphere-2025-318
Preprint. Discussion started: 24 January 2025

				et al. (2003)
Canopy height	h_c	m	[0.1, 10.0]	LAI allometric relationship from Jones (1998)
Leaf width	l_w	M	[0.01, 0.10]	Random, uniform distribution with global bounds
Leaf maximum carboxylation rate at 25 ºC	V_{cmo}	µmolC cm^{-2} m^{-1}	[0, 250]	PFT-dependent function of C_{ab} from Luo et al. (2019)
Leaf stomatal sensitivity (Ball Berry model slope)	m_{BB}	-	[1, 50]	Random, uniform distribution with PFT-dependent bounds from Miner et al. (2016)

2.2.4 Remote sensing and ecosystem functions emulators

For computational feasibility, BOSSE uses emulators (i.e., 2-hidden layer neural networks (Gómez-Dans et al., 2016)) of the Soil Canopy Observation, Photochemistry and Energy fluxes (SCOPE) model (Van Der Tol et al., 2009) to simulate RS imagery and most of the ecosystem functions (Table 2). The emulators predict hyperspectral *R*, hyperspectral *F*, and LST imagery as a function of plant traits, soil properties, meteorological data, and sun-view geometry (Supplementary Materials S4-S6). Additional emulators retrieve optical traits (RS-based estimates of plant traits) from sun angles and *R*, which can be also tailored to specific RS missions (i.e., EnMAP, DESIS, and Sentinel-2 MSI) by convolving first *R* to their spectral response functions. An additional emulator predicts gross primary production, evapotranspiration, transpiration, sensible heat and soil heat fluxes, net radiation, and total and green light-use efficiency; ecosystem respiration is approximated with the semi-empirical model of Migliavacca et al. (2011) and used to compute net ecosystem productivity. Additionally, BOSSE computes friction velocity for the later computation of ecosystem functional properties (Gomarasca et al., 2024)

Table 2. BOSSE remote sensing products and ecosystem functions variables

Parameter	Symbol	Units	Model	Features
Hyperspectral reflectance factors	*R*	-	SCOPE Emulator	1 nm step between 400 and 2500 nm
Sun-induced chlorophyll fluorescence radiance	*F*	mW m^{-2} sr^{-1} nm^{-1}	SCOPE Emulator	1 nm step between 641 and 849 nm
Land surface temperature	LST	K	SCOPE Emulator	Temperature Emissivity Separation (TES) algorithm
Optical traits	OT	various	SCOPE Emulator	N, C_{ab}, C_{ca}, C_{ant}, C_s, C_w, C_{dm}, $LIDF_a$, $LIDF_b$, LAI, h_c, and l_w

https://doi.org/10.5194/egusphere-2025-318
Preprint. Discussion started: 24 January 2025

Gross primary production	GPP	μmolC m^{-2} s^{-1}	SCOPE Emulator	
Total latent heat flux	λ	W m^{-2}	SCOPE Emulator	
Transpiration	λ_{canopy}	W m^{-2}	SCOPE Emulator	
Sensible heat flux	H	W m^{-2}	SCOPE Emulator	
Net radiation	R_n	W m^{-2}	SCOPE Emulator	
Soil heat flux	G_{tot}	W m^{-2}	SCOPE Emulator	
Light-use efficiency	LUE	μmolC μmol^{-1}	SCOPE Emulator	GPP / aPAR
Green light-use efficiency	LUE_{green}	μmolC μmol^{-1}	SCOPE Emulator	GPP / $aPAR_{green}$
Ecosystem respiration	R_{ECO}	μmolC m^{-2} s^{-1}	Semi-empirical model	(Migliavacca et al., 2011)
Ecosystem respiration at a reference temperature (15 ºC)	$R_{ECO,15C}$	μmolC m^{-2} s^{-1}	Semi-empirical model	(Migliavacca et al., 2011)
Net ecosystem productivity	NEP	μmolC m^{-2} s^{-1}	Equation	NEP = GPP - R_{ECO}
Friction velocity	u^*	m s^{-1}	Physical model	(Wallace and Verhoef, 2000)

The emulators were trained over a database of simulations generated with SCOPE 1.74 using the full model (including the energy balance and photosynthesis) to ensure that spectral variables were linked to the simulated plant physiology. Vegetation traits were randomly generated 1) using a GMM trained over a plant trait database (section 2.2.3) and 2) using a Latin Hypercube Sampling approach. Moreover, we developed a semi-parametric model (a 2D interpolator) predicting soil resistance for evaporation from the pore space as a function of the relative soil moisture (W_r, the ratio volumetric soil water content (SM_p) to soil field capacity (θ_{fc})) and a parameter determining the sensitivity of the response (Supplementary Material S5). Realistic meteorological conditions were randomly drawn from an additional GMM trained over a 10^5-size dataset subsampled from the BOSSE meteorological dataset (section 2.2.1).

The performance of the RS emulators and the effect on the derived functional diversity metrics (Table S6.1) were considered in line with the expected uncertainties of the different RS products. Similarly, the emulators' performance in predicting ecosystem functions was within the uncertainties expected from eddy covariance measurements (Table S6.2). While the emulators carry certain epistemic uncertainty, the underlying models also carry such uncertainty. As the models, the emulators establish sufficiently formal relationships between the plant traits and the RS variables used to estimate functional diversity metrics and the fluxes used to compute ecosystem functional properties, thus enabling the benchmark of methods exploring the relationships between those variables. BOSSE also allows adding random uncertainty to the simulated RS variables to match specific Gaussian noise levels.

https://doi.org/10.5194/egusphere-2025-318
Preprint. Discussion started: 24 January 2025

2.2.5 Phenological model

BOSSE uses the Growing Season Index (GSI) phenological model (Forkel et al., 2014) that defines vegetation phenology as a function of its response to light (i.e., incoming shortwave radiation), water availability, as well as cold and heat, determined by air temperature. GSI predicts vegetation trait values at any time as a function of the boundaries assigned to each pixel and meteorology (Supplementary Material S7). BOSSE assigns the PFT-dependent values parametrized by Forkel et al. (2014) and adds random Gaussian noise to generate variability between species and between traits. The GSI runs over the 30-day averaged meteorological values, and the rate of change of the GSI index is limited for each PFT to avoid unrealistic sudden changes in the vegetation state.

2.3 BOSSE initialization

2.3.1 BOSSE class initialization

The BOSSE class is initialized by passing two Python dictionaries containing the simulation options (Table 3) and paths necessary to load all the models and constants required and to store the outputs.

Table 3. BOSSE configuration arguments

Input	Data type	Default value	Meaning and values
"rseed_num"	integer	100	Seed for a random number generator. Controls the repeatability of the simulations
"subfolder_out"	string	"bosse_outputs"	Name of the subfolder where the different simulations are stored.
"scene_sz"	integer	60	Length in pixels of the Scene simulated.
"S_max"	integer	40	The maximum number of species that could be simulated in that Scene. A random number between "S_max" and 1 is selected in each case.
"sensor"	string	"Hy"	Name of the sensor that will be used to simulate spectral reflectance factors. BOSSE can ingest "Hy" (hyperspectral), which directly provides the 1-nm step output of the radiative transfer model between 400-2400 nm, "EnMAP" and "DESIS", which convolve the bands of the corresponding hyperspectral imagers and "S2", convolves reflectance factors to the bands of the Sentinel-2 multispectral imager.
"spat_res"	integer	100	Determines the spatial resolution of the sensor with respect to the plant size. 100 means that the plant and pixel feature the same size, and lower values equal the fraction of the plant to the pixel sizes in percentage values. For example, 50 indicates the pixel is two times larger than the

https://doi.org/10.5194/egusphere-2025-318
Preprint. Discussion started: 24 January 2025

			plant, and four plants can approximately be included in one pixel.
"sp_pattern"	string	"intermediate"	Patterns used to simulate the spatial distribution of species. "clustered" produces landscapes of grouped species; "even" leads to more scattered patterns, where species mix without forming closed clusters. "intermediate" is a mixture of both.
"clim_zone"	string	"continental"	The climatic zone where the simulated sites will be placed. It determines plant functional types and meteorological inputs. "Tropical", "Dry", "Temperate", and "Continental"
"inspect"	boolean	False	Option to inspect the results. If true, BOSSE produces different plots showing maps, meteorology, phenology, and plant traits of each site simulated.
"verbose"	boolean	False	Option to print information regarding the initialization and simulations.

During the initialization, BOSSE loads all the necessary datasets and models and preallocates 3D matrices representing the 2D Scene with the third dimension containing predefined values for all the plant, soil, and meteorological variables the model uses. BOSSE also establishes upper and lower bounds for each variable.

First, BOSSE sets the PFT-dependent information regarding:

1. The PFT and relative abundances corresponding to the selected climatic zone
2. The coefficients of the linear models relating V_{cmo} with C_{ab} from Luo et al. (2019) controlling photosynthesis and, therefore, fluorescence emission.
3. The Ball-Berry model slope (m_{BB}) ranges from Miner et al. (2016), controlling the ratio between photosynthesis and transpiration and, therefore, surface temperature.
4. Potential canopy conductance from Leuning et al. (2008).
5. PFT maximum leaf area index ($LAI_{max,PFT}$) values from Asner et al. (2003).
6. Parameters of the GSI phenological model from Forkel et al. (2014): which determine phenology and are used to filter the least adapted PFTs to local meteorology.
7. The ecosystem respiration model parameters and standard error from Migliavacca et al. (2011).

Next, it loads the following models:

1. The GMM used to draw random samples of correlated plant traits.
2. SCOPE model emulators to predict spectral signals (reflectance factors, fluorescence radiance, and land surface temperature), retrieve optical traits from canopy reflectance factors of different sensors, and predict ecosystem functions.
3. The model (a 2D interpolator) predicts soil resistance for evaporation from the pore space as a function of the W_r and a parameter determining the sensitivity of the response.

https://doi.org/10.5194/egusphere-2025-318
Preprint. Discussion started: 24 January 2025

2.3.2 BOSSE Scene initialization

Once BOSSE has loaded all the necessary variables and models, it can initialize a given Scene, which is controlled by the options provided when the BOSSE class is initialized (Table 3). The only necessary input argument is an integer number that identifies the meteorological dataset to be loaded. This number is used by default to seed the BOSSE class random number generators to ensure reproducibility; alternatively, the user can provide a different seed number and a low bound for the maximum mean LAI simulated in the Scene ($LAI_{max,Sc}$). By default, $LAI_{max,Sc} \geq 1.0$ m^2 m^{-2} to generate Scenes with a certain amount of vegetation. However, this value can be lowered to represent barely vegetated Scenes. The random number generator is seeded several times during the Scene initialization to maximize the comparability of the species' plant traits for the scenes generated with different spatial patterns.

2.3.2.1 Meteorological and leaf area index data

First, the time series of ERA5-Land meteorological variables are loaded for the site. Units are converted to those of the SCOPE model when necessary. Since ERA5-Land timestamps are UTC, the first and the last day might be incomplete in local time; therefore, these are gap-filled data from the nearby day, so they feature 24 hourly values at local time, which is the time used by BOSSE. Next, unfeasible negative values are interpolated and, if persistent, truncated. W_r, vapor pressure deficit, and timestamps in different formats (e.g., Day of the Year) are then computed. Finally, BOSSE calculates daily and 30-day averages and midday values and stores them in separate data frames; also, daily potential evapotranspiration is calculated using the Python package "pypyet" (Vremec et al., 2023) according to Penman-Monteith (1965).

2.3.2.2 Soil properties and climatic PFT filtering

The random number generator is seeded for the first time. Then, BOSSE randomly generates unique values of the SCOPE soil reflectance model parameters and field capacity (θ_{fc}, [-]) for the Scene. θ_{fc} is set within 100-150 % of the maximum volumetric moisture content (SM_p, [%]) of the time series, and water availability (W_r, [-]) is updated according to the new θ_{fc}. Next, BOSSE uses the default PFT-dependent parameters of the phenological model and W_r to calculate the GSI time series of each PFT, utilizing the default coefficient values from Forkel et al. (2014). BOSSE filters out the PFTs that are poorly adapted to the Scene's climate. To do so, it compares the percentile 95 (or 5 for the warm temperature) of each meteorological variable with the corresponding GSI "base" parameter that determines the inflection point of the phenological response function to meteorology (see Supplementary Material S7). BOSSE removes the PFTs from the Scene where the most extreme meteorological conditions do not cross this point, assuming these are too stressful for such species to develop in competition with other species. If no PFT meets these criteria, BOSSE keeps only the most competitive PFT (reaching the largest phenological index values).

2.3.2.3 Species location and correlation with soil properties

Then, some or all of the remaining PFTs are randomly selected for the Scene, and individuals of different species are assigned to the scene pixels. BOSSE runs at a 100 % spatial resolution; therefore, each pixel is occupied by a single phenotype (a single individual or identical individuals of the same species), meaning a unique set of vegetation parameters.

https://doi.org/10.5194/egusphere-2025-318
Preprint. Discussion started: 24 January 2025

The number of species is randomly sampled from the range between 1 and the input "S_max" (maximum species richness). BOSSE assigns these species to the PFTs and, together with foreseen relative abundances and the spatial pattern configured ("clustered", "intermediate", or "even"), the Neutral Landscape model (Etherington et al., 2015) distributes them in space. Neutral Landscape produces spatial patterns of a continuous variable that is then classified to determine the pixels belonging to each species, trying to respect the foreseen abundances, which must be recomputed later. BOSSE filters this spatial pattern generated using a Gaussian kernel of standard deviation randomly selected between [.5, 1.5] pixels. This smoothed map is then used to scale the soil reflectance model variables (B, lat, and lon), generating a spatial variability of soil properties that is partly correlated with the species' location.

2.3.2.4 Species functional traits

Plant trait values are randomly generated, either using the GMM for the leaf radiative transfer variables (N, C_{ab}, C_{ar}, C_{ant}, C_s, C_w, C_{dm}) or simply randomly sampling within predefined bounds ($LIDF_a$, $LIDF_b$, LAI, l_w, and m_{BB}) (Table 1). For each desired draw of plant traits, the GMM sampling is truncated between these bounds by discarding samples exceeding the bounds until the desired number of samples is generated. If the dataset cannot be completed (e.g., after ten attempts), a large set of samples is produced, and the values outside the bounds are randomly sampled within them. Since this could lead to unrealistic combinations of traits, only the samples with the largest plausibility (log-likelihood) are used to complete the dataset. Moreover, V_{cmo} is computed as a function of C_{ab} using PFT-dependent relationships from Luo et al. (2019), and canopy height (h_c) is computed using the allometric relationship with LAI and PFT-dependent scaling factors described in Jones (1998).

BOSSE determines the phenological maximum and minimum values for the plant traits per pixel, considering that the bounds of some plant traits are PFT-dependent (e.g., LAI, C_{ab}, and m_{BB}). For each PFT, BOSSE randomly generates a set of plant traits and a range of variability between the 10 % and the 40 % of the global PFT range. The ranges above and below this "central" value are used to generate random sets of mean plant traits for the species of each PFT (Fig. 2a). For each Scene, the interspecific variability is calculated from the weighted average of the plant traits of all the species included. Then, for each species, BOSSE calculates an intraspecific variability, assuming it ranges between 20 % and 40 % of the interspecific variability (Fig. 1 in Albert et al. (2010)) (Fig. 2b). Using each initial mean species plant trait values and the intraspecific variability, the plant traits of each species individual (i.e., pixel) are randomly determined. This process can bias the resulting species' mean from the initial mean value. Also, any value outside the global bounds of the above and below-average site ranges are truncated if they exceed the global trait bounds. Finally, each pixel's phenological maximum and minimum values are produced by adequately assigning the largest or the lowest value to the maximum or minimum phenological moment (Fig. 2c). For example, pigments and structural variables maximize in the green peak (GSI=1), but senescent pigments content (C_s) are assumed minimum during that period. Also, BOSSE ensures that LAI, C_{ab}, carotenoids (C_{ca}), and anthocyanins (C_{ant}) content of deciduous species equal zero at the bottom of the phenological period (GSI=0) and reduces the range of variability of all variables for the evergreen PFTs. It also ensures that the C_s only develop after the green peak (maximum GSI of the year). At any time (t) of the simulations, the plant trait values are determined by interpolating

https://doi.org/10.5194/egusphere-2025-318
Preprint. Discussion started: 24 January 2025

between these phenological bounds with the corresponding phenological state determined by the GSI. When LAI=0, plant traits are set to 0, which improves the emulators' performance.

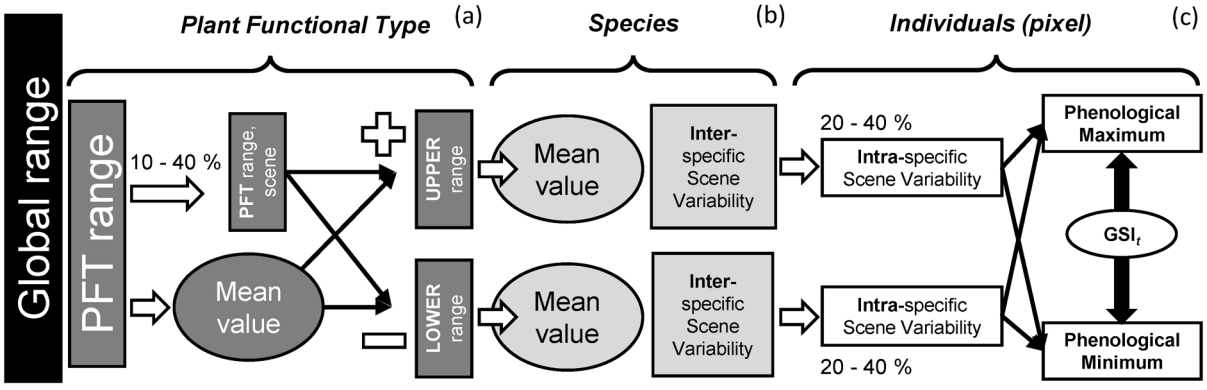

Figure 2: Generation of phenological maximum and minimum plant trait values for each plant individual (pixel).

2.3.2.5 Functional traits temporal variability

Then, the GSI phenological model is run using 30-day averages of the meteorological variables. Starting from the PFT parameter values, different parameters are generated for each species and plant trait by adding random Gaussian noise (5 % for the slope (s_{GSI}) and the base (b_{GSI}), and 1 % for the legacy sensitivity (τ_{GSI}), Supplementary S7). This allows species of the same PFT to behave similarly but prevents all the plant traits from synchronizing precisely.

BOSSE runs GSI using the incoming shortwave radiation and air temperature from ERA-5 Land. Following Forkel et al. (2014), water availability must be calculated from the relative soil water content, a PFT-defined maximum transpiration value (Table 1 in Gerten et al. (2004)), potential evapotranspiration, and a PFT-dependent potential canopy conductance value from Leuning et al. (2008). Since GSI is a dynamic model, the first 100 data points in the meteorological time series are reversed and added to the beginning of the series to circumvent the initial condition problem. A first run is executed with an initial GSI value equal to 0 to get a first guess of the GSI values. Then, the model is rerun using the GSI values at position 200 of the extended time series, which features the same meteorological conditions as the first point. The final GSI index, used to describe the phenology of each species, is the product of each of the individual indices representing the response to each of the drivers.

Moreover, to prevent unrealistically fast changes in the vegetation's phenological status, BOSSE includes some PFT-dependent arbitrary limits to the rate of change of the GSI index of each of the response functions of the model (Table S7.1). During the calculation of the GSI index, these values truncated any change of the index, taking into account the time step length of the change.

2.3.2.6 Ecosystem respiration model parameters

https://doi.org/10.5194/egusphere-2025-318
Preprint. Discussion started: 24 January 2025

BOSSE uses the model described and parametrized by Migliavacca et al. (2011) to predict ecosystem respiration (R_{eco}) and takes the PFT-dependent parameters and their associated standard errors reported in the abovementioned manuscript (Supplementary S8). The model scales R_{eco} with the maximum seasonal leaf area index, which is determined at this point for each pixel. This is done by multiplying the maximum species-dependent GSI value assigned to LAI and the LAI upper bound assigned to each pixel.

Then, for the rest of the model parameters, BOSSE first generates the interspecific variability by random sampling parameter values of a Gaussian distribution with a mean equal to the adjusted PFT-dependent value and standard deviation equal to the reported standard error in Table 5 in Migliavacca et al. (2011). Once the model parameters are defined per species, intraspecific variability is generated by adding random noise drawn from a uniform distribution, assuming traits' intraspecific variability ranges between 20 % and 40 % of the interspecific variability (Fig. 1 in Albert et al. (2010)).

2.4 BOSSE simulation

2.4.1 Trait maps

BOSSE uses the precomputed plant trait bounds and the GSI values to generate plant trait maps at any time (t) of the meteorological time series. Each species and trait GSI value ($GSI_{sp,PT} \in [0, 1]$) is used to linearly interpolate the corresponding trait value between the bounds corresponding to the upper (PT_{upper}) and lower (PT_{lower}) points of the phenology, assigned for each trait and pixel (pix) of the Scene (1). The fact that all the necessary variables are precomputed during initialization ensures the repetition of these simulations.

$$PT_{t,pix} = PT_{lower,pix} + \left(PT_{upper,pix} - PT_{lower,pix}\right) \cdot GSI_{t,sp,PT}\,, \quad (1)$$

2.4.2 Remote sensing imagery and products

BOSSE can simulate maps of plant traits and related RS imagery and products (R, F, LST, and OT) for any sample of the meteorological dataset. The phenological state (GSI value) is determined daily, and then the meteorological conditions and sun angles are set hourly. The hyperspectral reflectance factors (R, [-]) are initially generated at 1 nm step, between 400 and 2400 nm. These can be convolved to the spectral response functions of different RS imagers (EnMAP, DESIS, and Sentinel-2 MSI). Fluorescence radiances (F, [mW m^{-2} sr^{-2} nm^{-1}]) are also provided at 1 nm step between 641 and 849 nm, and land surface temperature (LST, [K]) is a single layer.

In addition, RS imagery spatial resolution can be downgraded using a Gaussian point spread function (PSF) model to more accurately mimic the spatial artifacts that can occur due to the gridding step that separates RS observations from the resulting gridded imagery (Wang et al., 2020; Duveiller et al., 2011) (Supplementary S9). A Gaussian PSF model is currently adopted (Eq. 3), aiming at considering the PSF effects only at nadir with an isotropic assumption. BOSSE spatial resolution (r_{spat}) is defined as the ratio of the simulation (plant) to the pixel size; therefore, a 100 % resolution implies that each pixel contains

https://doi.org/10.5194/egusphere-2025-318
Preprint. Discussion started: 24 January 2025

unmixed information of a unique individual or set of identical individuals. The resolution of the plant trait maps can also be degraded since many RS-related field campaigns use plots and not species as sampling units. In this case, BOSSE uses a simpler regular grid since the RS sampling process does not need to be simulated and is closer to how field data are gridded (e.g., Hauser et al. (2021)). This feature would allow assessing the effect of the RS sampling at different scales (with their respective PSF effects) to see if this "erases" our capacity to detect the underlying traits accordingly.

Finally, a different set of emulators can retrieve the vegetation traits (optical traits) from the simulated *R* images to include the effect of the retrieval uncertainty (noise and biases) in the analyses. This retrieval is performed with emulators trained independently from the emulators predicting *R* (Supplementary S9); moreover, these emulators have been trained for specific sets of spectral bands (i.e., hyperspectral and the missions EnMAP, DESIS, and Sentinel-2). The emulators can be applied to *R* with any (100 % or down-graded resolution), which also allows for assessing how the loss of spatial detail propagates to the estimated optical traits.

2.4.2 Ecosystem functions

BOSSE uses instantaneous meteorological data and vegetation and soil traits to predict instantaneous gross primary production (GPP), total latent heat flux (λE), canopy latent heat flux (λE_{canopy}), sensible heat flux (H), net radiation (R_n), soil heat flux (G), light use efficiency (LUE), and LUE computed with the photosynthetically active radiation absorbed by chlorophyll (LUE_{green}) using a SCOPE dedicated emulator. Negative GPP, LUE, and LUE_{green} are allowed to prevent biases in averages and ecosystem functional properties, which is acceptable since these values are present in observational datasets due to uncertainty. The analysis of the simulated fluxes might be subject to quality analysis and filtering, as the observations. In addition, R_{eco} is computed also using the model described in Migliavacca et al. (2011). The model is parametrized to predict daily R_{eco}, using daily mean air temperature, daily GPP, and monthly precipitation. Therefore, the model is fed with the values averaged for those periods around the timestamp where respiration is computed. R_{eco} is converted to μmolC m^{-2} s^{-1} to calculate net ecosystem productivity (NEP = GPP – R_{eco}); additionally, $R_{eco,15C}$ at the reference temperature of 15 C degrees is also computed. Finally, BOSSE also calculates the friction velocity (u^*) following Wallace and Verhoef (Wallace and Verhoef, 2000), as done in the SCOPE model. The ecosystem functions can be provided as a map or as the average value for the Scene.

3 Results

The pyBOSSE package features a “tutorial_bosse_v1_0.ipynb” Jupyter Notebook that shows how to import the pyBOSSE and pyGNDiv packages, and then initialize the BOSSE class, create Scenes with different features, retrieve the trait maps and the remote sensing products, visualize them, and compute functional diversity metrics on the maps and imagery. This section presents more advanced results (see “ManuscriptFigures.py”) that require the computation of time series in some cases, but the precomputed results are also provided.

https://doi.org/10.5194/egusphere-2025-318
Preprint. Discussion started: 24 January 2025

3.1 Scene spatial patterns and species distribution

BOSSE can represent Scenes featuring the same number of species with similar plant trait values (on average) but different spatial distributions to assess its impact on the assessment of plant diversity and its relationship with ecosystem functions, if any. Fig. 3a-c exemplifies the simulation of the same Scene species with three different spatial patterns: "clustered", "intermediate", and "even", respectively.

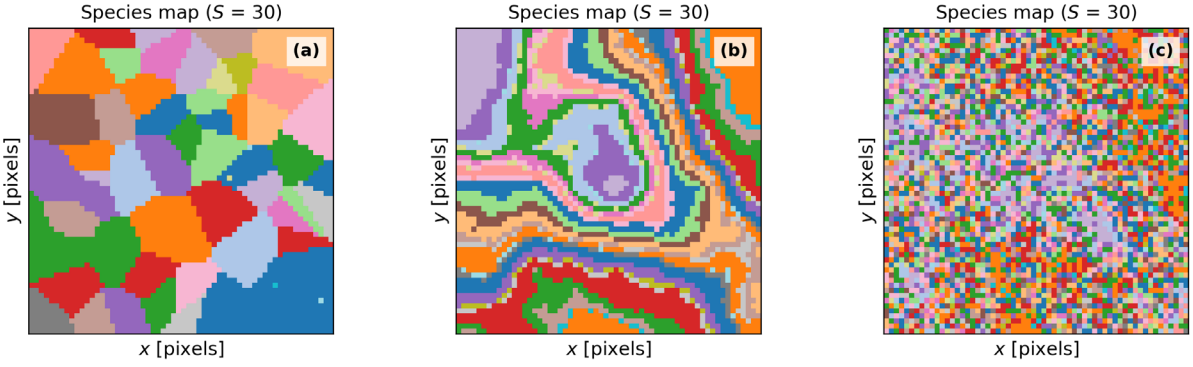

Figure 3: Simulation of a Scene with different spatial patterns: "clustered" (a), "intermediate" (b), and "even" (c). The number of species is the same for all the cases; however, the relative abundance and the averaged value of the plant traits per species can vary slightly.

3.2 Vegetation phenology, intra and inter-specific variability

BOSSE simulates the time series of vegetation functional traits associated with species' individuals. Fig. 4 exemplifies the simulated LAI (Fig. 4a-f) and leaf chlorophyll content (C_{ab}, Fig. 4g-l) for scenes in different climatic zones and spatial patterns (i.e., those in Fig. 3). Fig. 4 presents the mean and one standard deviation (σ) confidence interval for each species, colored by PFTs; species richness (S) is 30 in all the cases). For the same Scene, BOSSE ensures that the averaged values of each species are very similar across the spatial patterns (Fig. 4a-c,g-i); however, climatic conditions and local meteorology modify the PFTs and species included in each site, and therefore, their trait values (Fig. 4a,d-f,g,j-l). The different seasonalities of evergreen and deciduous species are clearly visible and change across climates; grasses respond faster to meteorological changes than the other PFTs.

https://doi.org/10.5194/egusphere-2025-318
Preprint. Discussion started: 24 January 2025

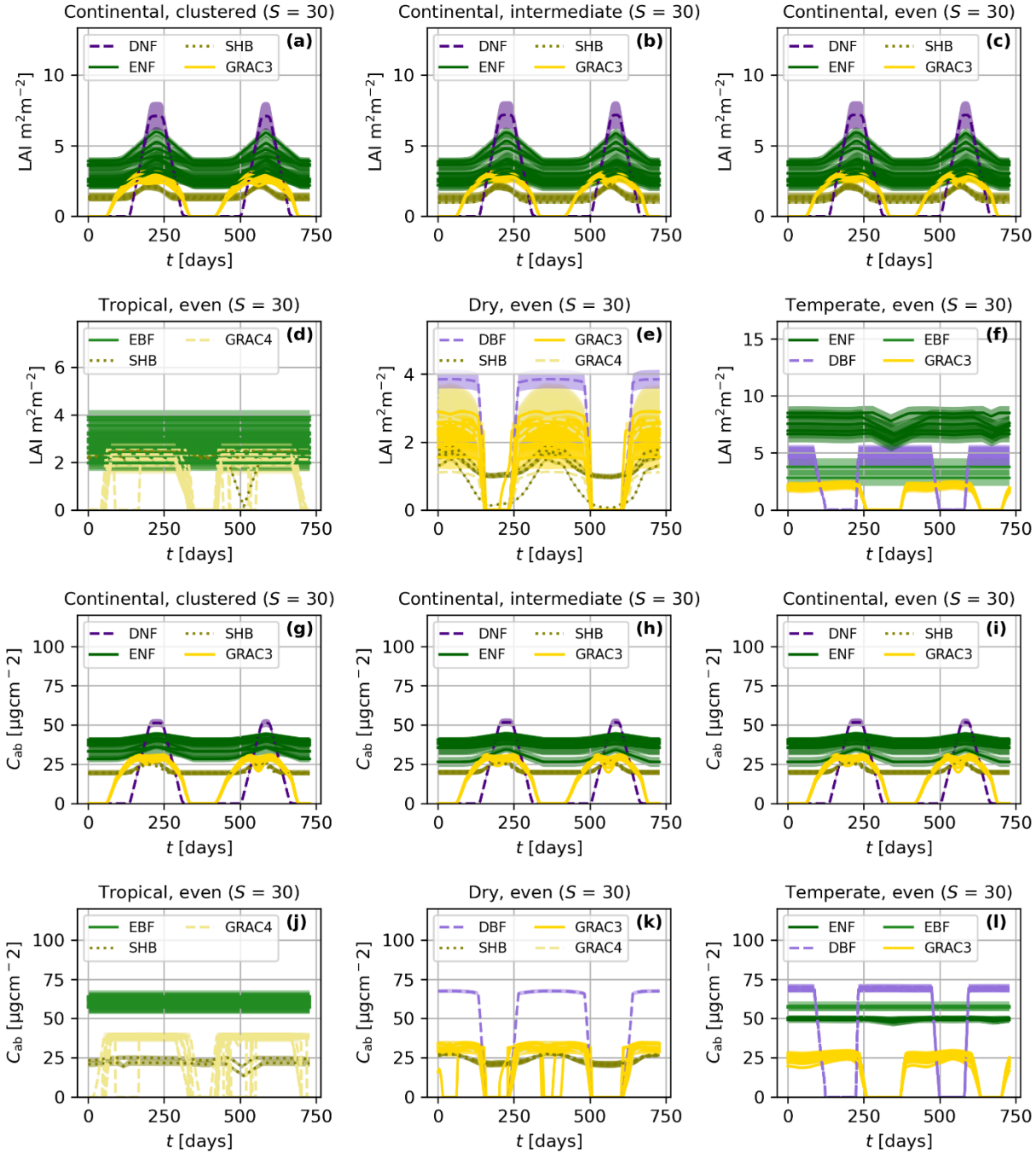

Figure 4: Time series of leaf area index (LAI, a-f) and leaf chlorophyll content (C_{ab}, g-l) for different spatial patterns (a-c,g-i) and climatic zones (a,d-f,g,j-l). The averaged value of the traits and one-standard deviation (σ) confidence interval are presented per each species. The colors represent the plant functional type of each species: deciduous broadleaf forest (DBF), evergreen broadleaf forest (EBF), shrubland (SHR), C3 grassland (GRAC3), and C4 grassland (GRAC4).

https://doi.org/10.5194/egusphere-2025-318
Preprint. Discussion started: 24 January 2025

3.3 Scene maps, vegetation properties, and remote sensing products

Fig. 5 exemplifies the simulation of Scene maps and RS products for an "intermediate" spatial pattern (see Fig. S10.1 and S10.2 for the "clustered" and "even" spatial pattern examples, respectively). The simulation takes place specifically at midday of day 230 of the time series presented in Fig. 4b,h, during the green peak. The species map (Fig. 5a) generated during the Scene initialization is the base to produce other maps at each timestamp. Each species is associated with a PFT (Fig. 5b). BOSSE first simulates the plant trait maps (e.g., LAI and C_{ab}, Fig. 4c-d) and, from those, simulates the remote sensing imagery. In this case, we computed the Normalized Difference Vegetation Index (Rouse et al., 1974) and the Near-infrared reflectance of vegetation (Badgley et al., 2017) spectral indices computed from the hyperspectral reflectance factors (Fig. 5e,f). The indices are coherent with the properties and taxonomy of vegetation. The figure also shows the fluorescence radiance at 687 and 760 nm from the hyperspectral spectra (Fig. 5i,j) and LST (Fig 5k), which include information about the physiological status of vegetation. In addition, BOSSE can retrieve optical traits (Fig. 5g-h), each estimated with different uncertainty (Fig. 5l). In this specific case, the retrieved LAI correlates well with the simulated one. In contrast, C_{ab} has been overestimated and is retrieved less accurately, which is not contrasting since foliar parameters are more challenging to retrieve (e.g., Pacheco-Labrador et al. (2024)). Overall, the RS images and optical traits follow the patterns presented by the vegetation traits with varying degrees of correlation. The previous relationships allow them to capture different PFD measures with various accuracy levels, alone or in combination. These correlations are the basis for assessing the capability of remote sensing to capture plant functional diversity.

https://doi.org/10.5194/egusphere-2025-318
Preprint. Discussion started: 24 January 2025

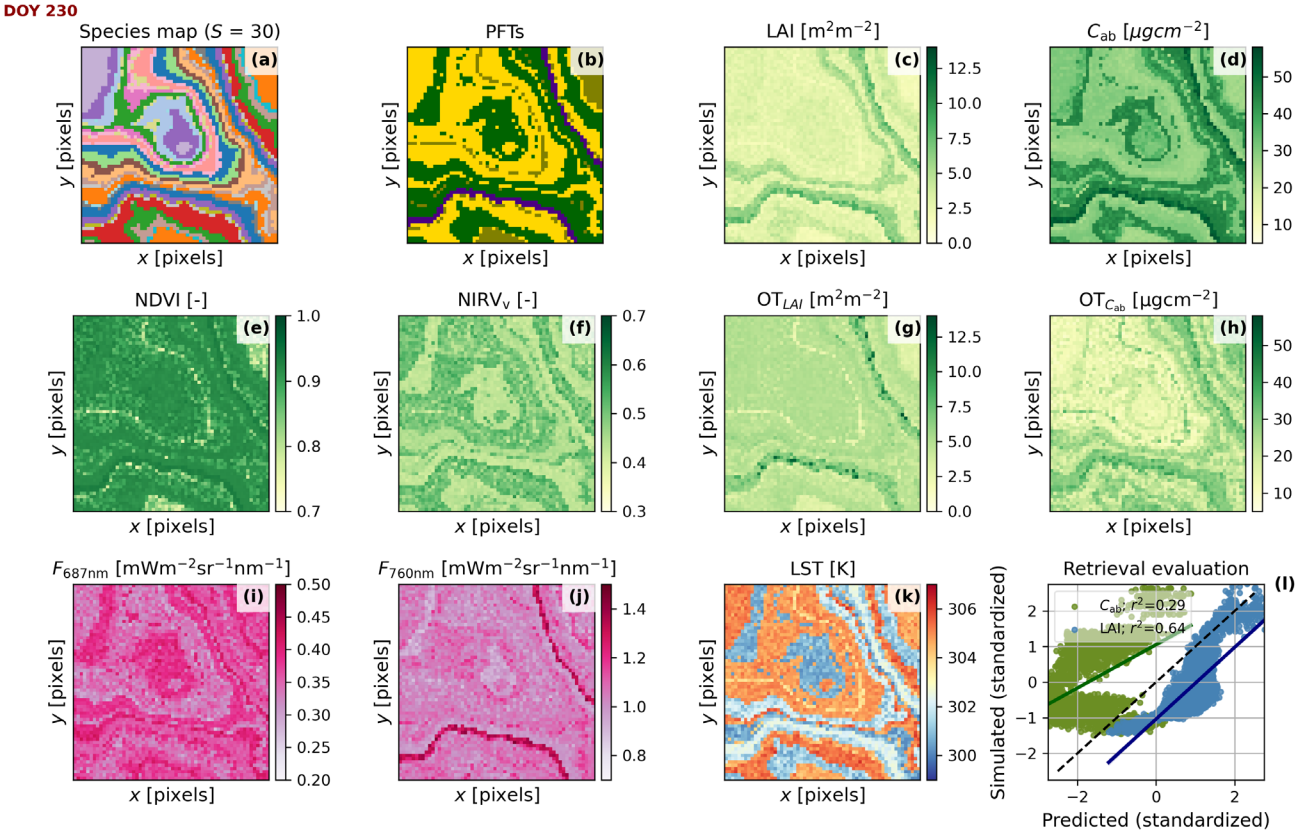

Figure 5: Simulated scene located in Continental climate and an "intermediate" spatial pattern at midday of day 230 of the time series presented in Fig. 4b,h. The coordinates are shown in pixels. Maps of species, indicating taxonomical Richness (*S*) (a), species' plant functional types (b), leaf area index (c), foliar chlorophyll content (d), normalized difference vegetation index (e), near-infrared reflectance of vegetation index (f), estimated leaf area index (g), estimated foliar chlorophyll content (h), fluorescence radiance at 687 nm (i), fluorescence radiance at 760 nm (j), land surface temperature (k), and the predicted vs. simulated leaf area index (c vs. g, blue) and foliar chlorophyll content (d vs. h, green) (l), standardized for the comparison and evaluated with the Pearson correlation coefficient (r^2).

3.4 Spatial resolution and functional diversity estimates

BOSSE can simulate remote sensing imagery at different relative spatial resolutions, defined as plant-to-pixel size ratio. As the resolution coarsens, it becomes suboptimal for diversity analysis as the signals of more and more different plants are integrated into a single pixel of the coarse-resolution simulated images. This feature can help analyze suboptimal resolution estimation of PFD, enabling users to test whether a given approach is robust to a specific spatial resolution. The spatial resolution has a strong effect on the computation of the diversity metrics as shown for Q_{Rao} (mean of 3 × 3 windows) and f_α estimated from $\mathrm{NIR_v}$ (Fig. 6a-e), F at 760 nm (Fig. 6f-j), and LST (Fig. 6l-o). The loss of spatial resolution can result in both positive or negative biases according to the underlying configuration. In this case ("intermediate" spatial pattern), both

https://doi.org/10.5194/egusphere-2025-318
Preprint. Discussion started: 24 January 2025

metrics (Q_{Rao} and f_α) seem to decrease when resolution reduces to 90 % and then increase, reaching values above the ones at the 100 % resolution as it continues degrading. The behavior is also found for the other spatial patterns of the same Scene (see Fig. S11.1 and S11.2 for the "clustered" and "even" spatial pattern examples, respectively).

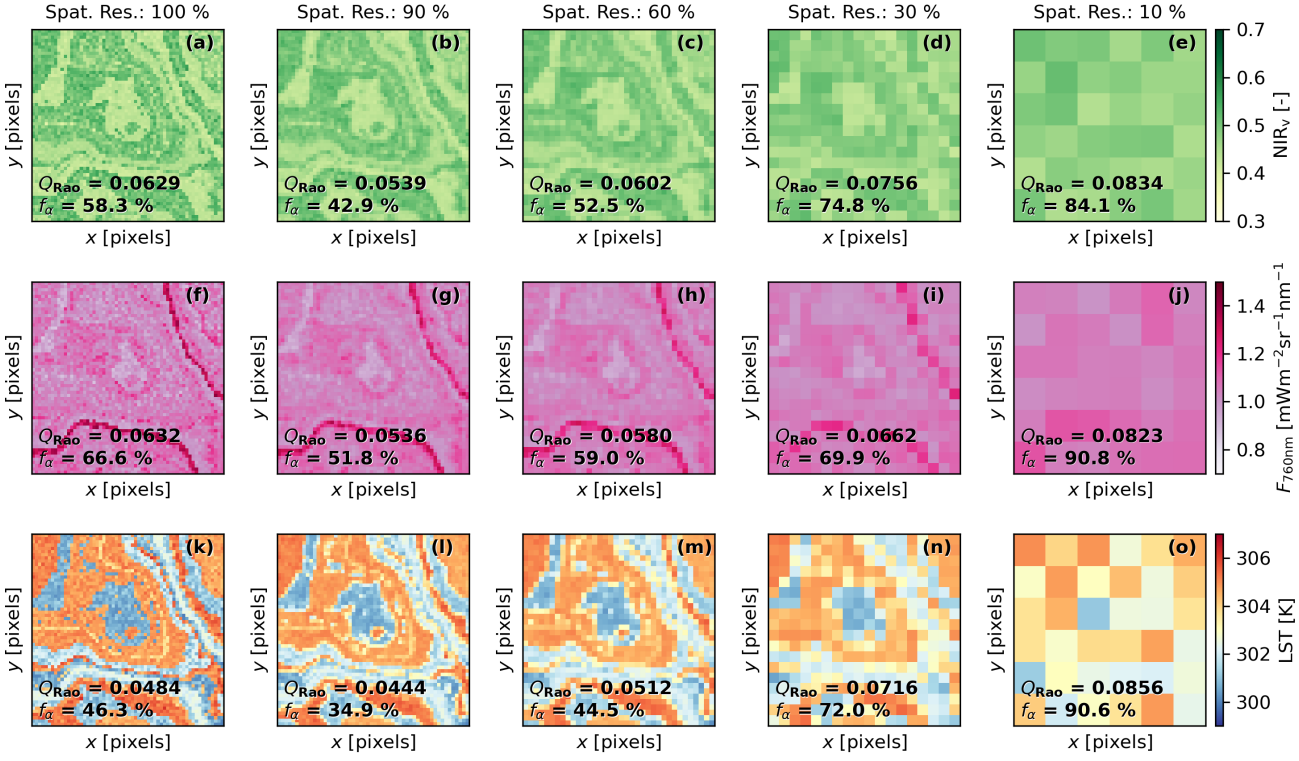

Figure 6: Simulated imagery of the near-infrared of vegetation index (a-e), fluorescence radiance at 760 nm (f-j), and land surface temperature (l-o) using an "intermediate" spatial pattern at different spatial resolutions (100%, 90%, 60%, 30%, and 10%), defined as the plant-to-pixel size ratio. The mean value of Rao's quadratic entropy (Q_{Rao}) calculated over a 3 × 3 pixels moving window and the fraction of α-diversity (f_α), calculated from the variance-based partition approach, are presented for each map. The coordinates are shown in pixels.

3.5 Ecosystem function time series

BOSSE can compute different ecosystem functions at hourly timestamps. Fig. 6 shows the integrated functions corresponding to the Scene represented in Fig. 4b and Fig. 5 for two years. In this case, the functions are computed per pixel and averaged for the whole Scene. The fluxes follow the expected seasonal behavior, following the Scene meteorology (Fig. S12), featuring one productive peak per year.

https://doi.org/10.5194/egusphere-2025-318
Preprint. Discussion started: 24 January 2025

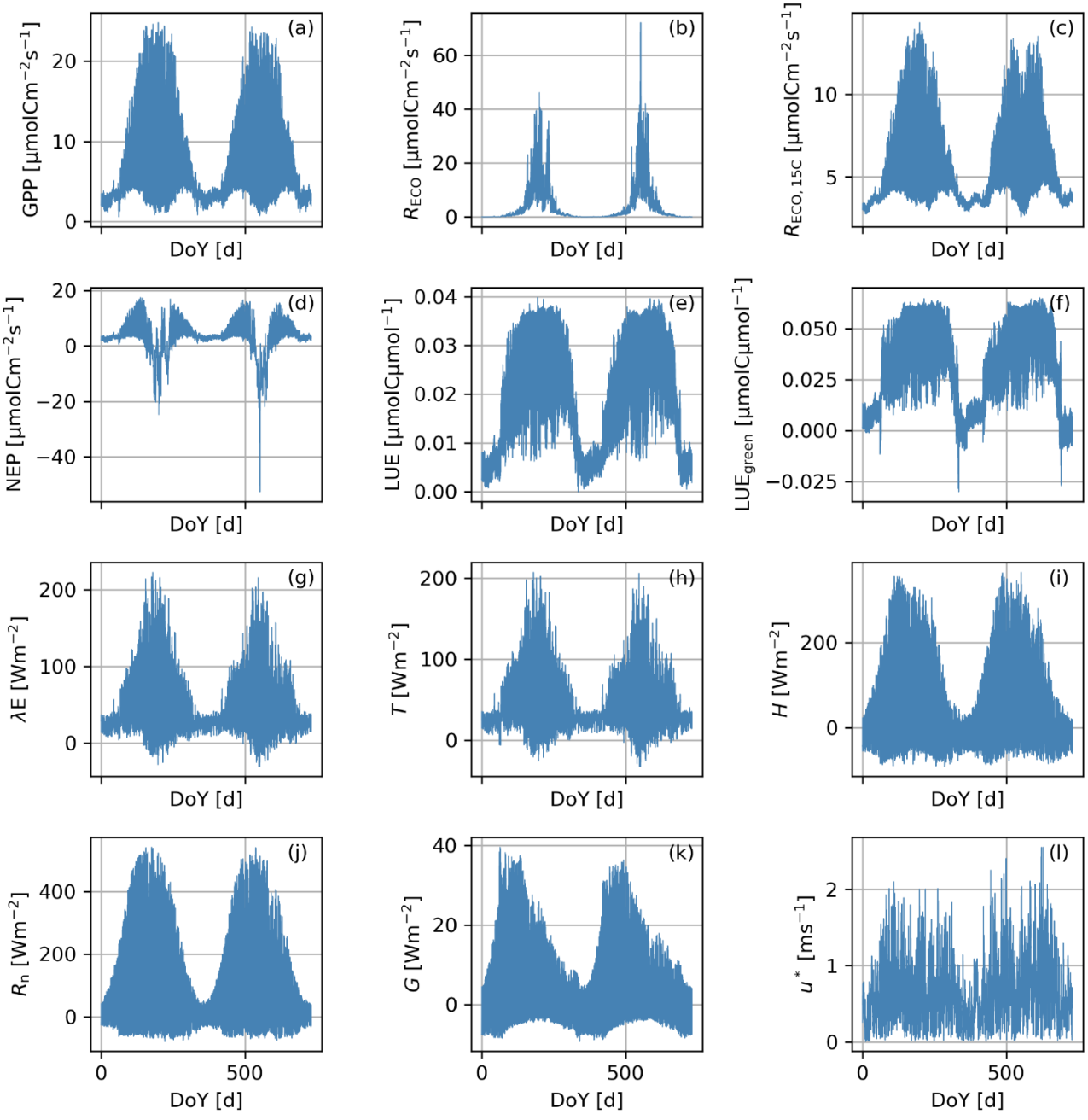

Figure 7: Time series of Scene-integrated ecosystem functions corresponding to a Scene simulated in a Continental climatic zone with an "intermediate" pattern: gross primary production (a), ecosystem respiration (b), ecosystem respiration at 15ºC (c), net ecosystem productivity (d), light use efficiency (e), green light use efficiency (f), latent heat flux (g)), transpiration (h), sensible heat fluxes (i), net radiation (j), soil heat fluxes (k), and friction velocity (l).

https://doi.org/10.5194/egusphere-2025-318
Preprint. Discussion started: 24 January 2025

4 Discussion

BOSSE is the first Observing System Simulation Experiment (OSSE) dedicated to studying plant diversity from RS. Simulations have been recently applied to tackle methodological questions regarding the remote estimation of different aspects of plant diversity (Pacheco-Labrador et al., 2022; Pacheco-Labrador et al., 2023; Gomarasca et al., 2024; Fassnacht et al., 2022; Ludwig et al., 2024). However, none of these works have provided a sufficiently comprehensive tool to spatially describe different ecosystem types and landscapes in various climatic zones across time. Also, while simulations of all these works have explored the links between spectral and plant diversity, none of them has aimed to explore simulated BEF relationships derived from RS. BOSSE also simulates additional spectral signals beyond vegetation reflectance factors (i.e., SIF and LST), which might help elucidate these signals' potential contribution to the study of plant diversity or BEF analyses.

Despite the inherent limitations of the simulations, these are still necessary tools to clarify fundamental questions in this emerging research field. The lack of global comparable field data sets acquired for validating RS estimates of plant diversity hampers the definition and selection of reliable metrics and methodologies. This is particularly relevant for the analysis of functional diversity, where noise and uncertainty can be confounded with variability. Using simulations, Pacheco-Labrador et al. (2022) showed that some functional diversity metrics presented a large variability of performances when used at local scales (e.g., a single study site) or were prone to spuriousness under uncertainty. Therefore, the empirical results of local studies might not be sufficient to identify the most reliable methodologies, and their publication might suffer from a survivorship bias not necessarily related to the capability of approaches and metrics to capture plant functional diversity from RS. Furthermore, the SVH on which the assessment of plant diversity from remote sensing relies has been questioned (Torresani et al., 2024), and modeling and observational works have identified significant limitations (Ludwig et al., 2024; Pacheco-Labrador et al., 2022; Fassnacht et al., 2022; Wang et al., 2018). It could be that SVH is not applicable in practice or that we have not yet found reliable methodologies and the limits of their application; considering the limitations of comparable field measurements and local studies, BOSSE and similar tools might play a fundamental role in the assessment of SVH. BOSSE aims not to replace the necessary field studies but to offer a framework to answer methodological questions that improve and guide the analysis of RS imagery and validate the estimates with real-world observations.

BOSSE simultaneously simulates species and plant trait maps, the associated remote sensing signals, and the related ecosystem functions. The quality of this information can be degraded at will to test the robustness or applicability of different methodologies capturing plant diversity and BEF relationships. BOSSE relies on emulators, accepting a certain degree of epistemic uncertainty between the original model and BOSSE simulations. However, these uncertainties might not differ too much from those existing between models and reality and still offer a systematic link between the variables of interest that allows testing whether different methodologies can capture and under which circumstances. While the relationships found between BOSSE variables could not be directly transferable to real-world applications (e.g., a relationship between Q_{Rao} computed from R and PT), BOSSE could help to define how plant diversity or BEF relationships

https://doi.org/10.5194/egusphere-2025-318
Preprint. Discussion started: 24 January 2025

should be estimated (e.g., selecting the most convenient moving window sizes), and how to adapt the methodologies to different sensors (spatial resolution, spectral configuration), or observational limitations, and organize field campaigns for validation. Still, in the case of plant functional diversity, simulations have provided results close to those found with observations (e.g., Pacheco-Labrador et al. (2022)). BOSSE phenology will also help to understand the role of vegetation phenological status on the reliability of diversity estimates or how to exploit this temporal information in the assessment of BEF relationships (which, so far, relies on the productive stages, e.g., Gomarasca et al. (2024)).

BOSSE v1.0 offers realistic simulations but also has excellent potential to increase their complexity and completeness and tackle more challenging questions in upcoming versions. The current version already allows for testing numerous fundamental but unsolved methodological questions about how spatial resolution, phenology, and different spectral signals affect or enable the estimation of plant functional diversity. BOSSE v1.0 is already the first simulation environment providing not only reflectance factors but also other signals of interest for studying plant diversity, such as SIF (Tagliabue et al., 2020) or the less explored LST, two signals related to vegetation physiology and ecosystem functions whose role on BEF analyses remains untested. In its current state, BOSSE v1.0 might help to test and improve methodologies already developed to characterize different aspects of plant diversity (e.g., Féret and De Boissieu (2020), Laliberté et al. (2020), Rocchini et al. (2021), Rossi et al. (2023), or Rossi et al. (2021)), and BEF relationships (Gomarasca et al., 2024).

BOSSE relies on 1D radiative transfer models representing vertically homogeneous canopies. Future versions could rely on more complex radiative transfer models representing vertically heterogeneous canopies (e.g., SCOPE 2 (Yang et al., 2021) or DART (Gastellu-Etchegorry et al., 2017)) and simulating LiDAR datasets, which could help to develop the capability of RS to infer plant diversity in structurally complex ecosystems where different species overlap (Almeida et al., 2021; Zhao et al., 2018). Radar imagery has also been proposed as a tool to assess vegetation diversity (Bae et al., 2019; Hoffmann et al., 2022); BOSSE v1.0 could also incorporate Radar radiative transfer models (e.g., Oh and Kweon (2013)) to assess the capabilities of this signal. Future BOSSE versions will include multi-angular capabilities to offer more realistic RS simulations of different sensors. BOSSE will also improve the representation of vegetation and its processes. Upcoming versions will also represent plants of different sizes and include more ecological theory, allowing for the competition and replacement of species, one of the key mechanisms behind the role of plant diversity on ecosystem stability (De Bello et al., 2021). While some models already present some of the features to be included in BOSSE (e.g., FORMIND represents vegetation interactions vertically heterogeneous canopies and features a LiDAR simulator (Knapp et al., 2018)), BOSSE aspires to provide more diverse features at a fast computational speed.

Beyond the study of plant diversity, BOSSE could support methodological development and benchmarking in other RS applications, particularly in those dealing with coarse spatial resolutions and integrating multiple RS products, or address scaling issues in surface-atmosphere flux modeling with low- or mid-resolution RS data. BOSSE could also support the development of digital tweens of existing landscapes via the assimilation of remote sensing and other observables.

https://doi.org/10.5194/egusphere-2025-318
Preprint. Discussion started: 24 January 2025

5 Conclusions

BOSSE is the first Observing System Simulation Experiment dedicated to studying plant diversity and biodiversity-ecosystem function relationships from remote sensing. It aims to support the development of these areas, overcoming the lack of global and consistent field datasets. In its first version, BOSSE will allow researchers to test hypotheses and benchmark methodologies, while future versions will grow in complexity to help answer more nuanced and diverse research questions. BOSSE will allow researchers to select the most promising approaches, test them with real-world observations, and interpret the results by characterizing the sensitivity of the methods to different confounding factors under controlled conditions. In addition, the spatial and temporal nature of BOSSE simulations could be used for the development of other remote sensing applications. We expect BOSSE and similar modeling approaches will contribute to elucidating whether and under which circumstances the Spectral Variation Hypothesis can be reliably applied or under which circumstances.

Code availability

The model pyBOSSE can be found at https://github.com/JavierPachecoLabrador/pyBOSSE. The latest version of pyGNDiv package, updated for faster computation and image analysis, can be found at https://github.com/JavierPachecoLabrador/pyGNDiv-master.

Data availability

The ERA5-Land hourly meteorological datasets required to run BOSSE at various locations can be found in https://doi.org/10.5281/zenodo.14717038 under Creative Commons Attribution 4.0 International license

Author contributions

JPL, UG, DEPM, WL, MM, and GD conceptualized and developed the methodology. JPL, GD, and MJ obtained the funding, JPL took care of data curation, software, and visualization. JPL and the co-authors prepared the manuscript draft.

Competing interests

The contact author has declared that none of the authors has any competing interests.

https://doi.org/10.5194/egusphere-2025-318
Preprint. Discussion started: 24 January 2025

Disclaimer

Acknowledgments

We thank Uli Weber, Daniel Loos, and Héctor Nieto for their support, discussions, and recommendations.

Financial support

BOSSE was developed under the ESA Living Planet Fellowship IRS4BEF (ESA Contract No. 4000140028/22/I-DT-lr), a programme of and funded by the European Space Agency. JPL acknowledges the project "Integrated Observing Systems and Simulation Experiments to Analyze Biodiversity-Ecosystem Function Relationships in Savanna Ecosystems" PID2023-151046NB-I00 funded by MCIU/ AEI / 10.13039/501100011033 / FEDER, UE). GD acknowledges funding from the European Research Council (ERC) Synergy Grant "Understanding and modeling the Earth System with Machine Learning (USMILE)" under the EU Horizon 2020 research and innovation program (grant agreement no. 855187).

References

Albert, C. H., Thuiller, W., Yoccoz, N. G., Douzet, R., Aubert, S., and Lavorel, S.: A multi-trait approach reveals the structure and the relative importance of intra- vs. interspecific variability in plant traits, Functional Ecology, 24, 1192-1201, https://doi.org/10.1111/j.1365-2435.2010.01727.x, 2010.

Almeida, D. R. A. d., Broadbent, E. N., Ferreira, M. P., Meli, P., Zambrano, A. M. A., Gorgens, E. B., Resende, A. F., de Almeida, C. T., do Amaral, C. H., Corte, A. P. D., Silva, C. A., Romanelli, J. P., Prata, G. A., de Almeida Papa, D., Stark, S. C., Valbuena, R., Nelson, B. W., Guillemot, J., Féret, J.-B., Chazdon, R., and Brancalion, P. H. S.: Monitoring restored tropical forest diversity and structure through UAV-borne hyperspectral and lidar fusion, Remote Sensing of Environment, 264, 112582, https://doi.org/10.1016/j.rse.2021.112582, 2021.

Asner, G. P., Scurlock, J. M. O., and A. Hicke, J.: Global synthesis of leaf area index observations: implications for ecological and remote sensing studies, Global Ecology and Biogeography, 12, 191-205, https://doi.org/10.1046/j.1466-822X.2003.00026.x, 2003.

Badgley, G., Field, C. B., and Berry, J. A.: Canopy near-infrared reflectance and terrestrial photosynthesis, Science Advances, 3, e1602244, 10.1126/sciadv.1602244, 2017.

Badourdine, C., Féret, J.-B., Pélissier, R., and Vincent, G.: Exploring the link between spectral variance and upper canopy taxonomic diversity in a tropical forest: influence of spectral processing and feature selection, Remote Sensing in Ecology and Conservation, 9, 235-250, https://doi.org/10.1002/rse2.306, 2023.

Bae, S., Levick, S. R., Heidrich, L., Magdon, P., Leutner, B. F., Wöllauer, S., Serebryanyk, A., Nauss, T., Krzystek, P., Gossner, M. M., Schall, P., Heibl, C., Bässler, C., Doerfler, I., Schulze, E.-D., Krah, F.-S., Culmsee, H., Jung, K., Heurich, M., Fischer, M., Seibold, S., Thorn, S., Gerlach, T., Hothorn, T., Weisser, W. W., and Müller, J.: Radar vision in the mapping of forest biodiversity from space, Nature Communications, 10, 4757, 10.1038/s41467-019-12737-x, 2019.

Barnett, D. T., Adler, P. B., Chemel, B. R., Duffy, P. A., Enquist, B. J., Grace, J. B., Harrison, S., Peet, R. K., Schimel, D. S., Stohlgren, T. J., and Vellend, M.: The plant diversity sampling design for The National Ecological Observatory Network, Ecosphere, 10, e02603, https://doi.org/10.1002/ecs2.2603, 2019.

Botta-Dukát, Z.: Rao's quadratic entropy as a measure of functional diversity based on multiple traits, Journal of Vegetation Science, 16, 533-540, https://doi.org/10.1111/j.1654-1103.2005.tb02393.x, 2005.

https://doi.org/10.5194/egusphere-2025-318
Preprint. Discussion started: 24 January 2025

Cavender-Bares, J., Gamon, J. A., Hobbie, S. E., Madritch, M. D., Meireles, J. E., Schweiger, A. K., and Townsend, P. A.: Harnessing plant spectra to integrate the biodiversity sciences across biological and spatial scales, American Journal of Botany, 104, 966-969, 10.3732/ajb.1700061, 2017.

Croft, H., Chen, J. M., Luo, X., Bartlett, P., Chen, B., and Staebler, R. M.: Leaf chlorophyll content as a proxy for leaf photosynthetic capacity, Global Change Biology, 23, 3513-3524, 10.1111/gcb.13599, 2017.

de Bello, F., Lavorel, S., Hallett, L. M., Valencia, E., Garnier, E., Roscher, C., Conti, L., Galland, T., Goberna, M., Májeková, M., Montesinos-Navarro, A., Pausas, J. G., Verdú, M., E-Vojtkó, A., Götzenberger, L., and Lepš, J.: Functional trait effects on ecosystem stability: assembling the jigsaw puzzle, Trends in Ecology & Evolution, 36, 822-836, https://doi.org/10.1016/j.tree.2021.05.001, 2021.

Dupré, J.: In defence of classification, Studies in History and Philosophy of Science Part C: Studies in History and Philosophy of Biological and Biomedical Sciences, 32, 203-219, https://doi.org/10.1016/S1369-8486(01)00003-6, 2001.

Duveiller, G., Baret, F., and Defourny, P.: Crop specific green area index retrieval from MODIS data at regional scale by controlling pixel-target adequacy, Remote Sensing of Environment, 115, 2686-2701, https://doi.org/10.1016/j.rse.2011.05.026, 2011.

Etherington, T. R., Holland, E. P., and O'Sullivan, D.: NLMpy: a python software package for the creation of neutral landscape models within a general numerical framework, Methods in Ecology and Evolution, 6, 164-168, https://doi.org/10.1111/2041-210X.12308, 2015.

Fassnacht, F. E., Müllerová, J., Conti, L., Malavasi, M., and Schmidtlein, S.: About the link between biodiversity and spectral variation, Applied Vegetation Science, 25, e12643, https://doi.org/10.1111/avsc.12643, 2022.

Féret, J.-B. and de Boissieu, F.: biodivMapR: An r package for α- and β-diversity mapping using remotely sensed images, Methods in Ecology and Evolution, 11, 64-70, https://doi.org/10.1111/2041-210X.13310, 2020.

Forkel, M., Carvalhais, N., Schaphoff, S., v. Bloh, W., Migliavacca, M., Thurner, M., and Thonicke, K.: Identifying environmental controls on vegetation greenness phenology through model–data integration, Biogeosciences, 11, 7025-7050, 10.5194/bg-11-7025-2014, 2014.

Gastellu-Etchegorry, J. P., Lauret, N., Yin, T., Landier, L., Kallel, A., Malenovský, Z., Bitar, A. A., Aval, J., Benhmida, S., Qi, J., Medjdoub, G., Guilleux, J., Chavanon, E., Cook, B., Morton, D., Chrysoulakis, N., and Mitraka, Z.: DART: Recent Advances in Remote Sensing Data Modeling With Atmosphere, Polarization, and Chlorophyll Fluorescence, IEEE Journal of Selected Topics in Applied Earth Observations and Remote Sensing, 10, 2640-2649, 10.1109/JSTARS.2017.2685528, 2017.

Gerten, D., Schaphoff, S., Haberlandt, U., Lucht, W., and Sitch, S.: Terrestrial vegetation and water balance—hydrological evaluation of a dynamic global vegetation model, Journal of Hydrology, 286, 249-270, https://doi.org/10.1016/j.jhydrol.2003.09.029, 2004.

Gomarasca, U., Duveiller, G., Pacheco-Labrador, J., Ceccherini, G., Cescatti, A., Girardello, M., Nelson, J. A., Reichstein, M., Wirth, C., and Migliavacca, M.: Satellite remote sensing reveals the footprint of biodiversity on multiple ecosystem functions across the NEON eddy covariance network, Environmental Research: Ecology, 3, 045003, 10.1088/2752-664X/ad87f9, 2024.

Gómez-Dans, J. L., Lewis, P. E., and Disney, M.: Efficient Emulation of Radiative Transfer Codes Using Gaussian Processes and Application to Land Surface Parameter Inferences, Remote Sensing, 8, 119, 2016.

Gonzalez, A., Vihervaara, P., Balvanera, P., Bates, A. E., Bayraktarov, E., Bellingham, P. J., Bruder, A., Campbell, J., Catchen, M. D., Cavender-Bares, J., Chase, J., Coops, N., Costello, M. J., Czúcz, B., Delavaud, A., Dornelas, M., Dubois, G., Duffy, E. J., Eggermont, H., Fernandez, M., Fernandez, N., Ferrier, S., Geller, G. N., Gill, M., Gravel, D., Guerra, C. A., Guralnick, R., Harfoot, M., Hirsch, T., Hoban, S., Hughes, A. C., Hugo, W., Hunter, M. E., Isbell, F., Jetz, W., Juergens, N., Kissling, W. D., Krug, C. B., Kullberg, P., Le Bras, Y., Leung, B., Londoño-Murcia, M. C., Lord, J.-M., Loreau, M., Luers, A., Ma, K., MacDonald, A. J., Maes, J., McGeoch, M., Mihoub, J. B., Millette, K. L., Molnar, Z., Montes, E., Mori, A. S., Muller-Karger, F. E., Muraoka, H., Nakaoka, M., Navarro, L., Newbold, T., Niamir, A., Obura, D., O'Connor, M., Paganini, M., Pelletier, D., Pereira, H., Poisot, T., Pollock, L. J., Purvis, A., Radulovici, A., Rocchini, D., Roeoesli, C., Schaepman, M., Schaepman-Strub, G., Schmeller, D. S., Schmiedel, U., Schneider, F. D., Shakya, M. M., Skidmore, A., Skowno, A. L., Takeuchi, Y., Tuanmu, M.-N., Turak, E., Turner, W., Urban, M. C., Urbina-Cardona, N., Valbuena, R., Van de Putte, A., van Havre, B., Wingate, V. R., Wright, E., and Torrelio, C. Z.: A global biodiversity observing system to unite monitoring and guide action, Nature Ecology & Evolution, 7, 1947-1952, 10.1038/s41559-023-02171-0, 2023.

https://doi.org/10.5194/egusphere-2025-318
Preprint. Discussion started: 24 January 2025

Harper, K. L., Lamarche, C., Hartley, A., Peylin, P., Ottlé, C., Bastrikov, V., San Martín, R., Bohnenstengel, S. I., Kirches, G., Boettcher, M., Shevchuk, R., Brockmann, C., and Defourny, P.: A 29-year time series of annual 300 m resolution plant-functional-type maps for climate models, Earth Syst. Sci. Data, 15, 1465-1499, 10.5194/essd-15-1465-2023, 2023.

Hauser, L. T., Féret, J.-B., An Binh, N., van der Windt, N., Sil, Â. F., Timmermans, J., Soudzilovskaia, N. A., and van Bodegom, P. M.: Towards scalable estimation of plant functional diversity from Sentinel-2: In-situ validation in a heterogeneous (semi-)natural landscape, Remote Sensing of Environment, 262, 112505, https://doi.org/10.1016/j.rse.2021.112505, 2021.

Hernández-Blanco, M., Costanza, R., Chen, H., deGroot, D., Jarvis, D., Kubiszewski, I., Montoya, J., Sangha, K., Stoeckl, N., Turner, K., and van 't Hoff, V.: Ecosystem health, ecosystem services, and the well-being of humans and the rest of nature, Global Change Biology, 28, 5027-5040, https://doi.org/10.1111/gcb.16281, 2022.

Hoffmann, J., Muro, J., and Dubovyk, O.: Predicting Species and Structural Diversity of Temperate Forests with Satellite Remote Sensing and Deep Learning, 10.3390/rs14071631, 2022.

Huntzinger, D. N., Schwalm, C. R., Wei, Y., Shrestha, R., Cook, R. B., Michalak, A. M., Schafer, K. V. R., Jacobson, A. R., Arain, M. A., Ciais, P., Fisher, B. D., Kolus, H., Sikka, M., Elshorbany, Y., Hayes, D. J., Huang, M., Huang, S., Ito, A., Jain, A. K., Lei, H., Lu, C., Maignan, F., Mao, J., Parazoo, N. C., Peng, C., Peng, S., Poulter, B., Ricciuto, D. M., Tian, H., Shi, X., Wang, W., Zeng, N., Zhao, F., Zhu, Q., Yang, J., and Tao, B.: NACP MsTMIP: Global 0.5-degree Model Outputs in Standard Format, Version 2.0, 10.3334/ORNLDAAC/1599, 2021.

Isbell, F., Calcagno, V., Hector, A., Connolly, J., Harpole, W. S., Reich, P. B., Scherer-Lorenzen, M., Schmid, B., Tilman, D., van Ruijven, J., Weigelt, A., Wilsey, B. J., Zavaleta, E. S., and Loreau, M.: High plant diversity is needed to maintain ecosystem services, Nature, 477, 199-202, 10.1038/nature10282, 2011.

Jones, C. P.: Ancillary file generation for the UM, Unified Model Documentation Paper #73, Met Office Technical Documentation, 1998.

Kattenborn, T., Schiefer, F., Zarco-Tejada, P., and Schmidtlein, S.: Advantages of retrieving pigment content [µg/cm2] versus concentration [%] from canopy reflectance, Remote Sensing of Environment, 230, 111195, https://doi.org/10.1016/j.rse.2019.05.014, 2019.

Kattge, J. and Bönisch, G. and Díaz, S. and Lavorel, S. and Prentice, I. C. and Leadley, P. and Tautenhahn, S. and Werner, G. D. A. and Aakala, T. and Abedi, M. and Acosta, A. T. R. and Adamidis, G. C. and Adamson, K. and Aiba, M. and Albert, C. H. and Alcántara, J. M. and Alcázar C, C. and Aleixo, I. and Ali, H. and Amiaud, B. and Ammer, C. and Amoroso, M. M. and Anand, M. and Anderson, C. and Anten, N. and Antos, J. and Apgaua, D. M. G. and Ashman, T.-L. and Asmara, D. H. and Asner, G. P. and Aspinwall, M. and Atkin, O. and Aubin, I. and Baastrup-Spohr, L. and Bahalkeh, K. and Bahn, M. and Baker, T. and Baker, W. J. and Bakker, J. P. and Baldocchi, D. and Baltzer, J. and Banerjee, A. and Baranger, A. and Barlow, J. and Barneche, D. R. and Baruch, Z. and Bastianelli, D. and Battles, J. and Bauerle, W. and Bauters, M. and Bazzato, E. and Beckmann, M. and Beeckman, H. and Beierkuhnlein, C. and Bekker, R. and Belfry, G. and Belluau, M. and Beloiu, M. and Benavides, R. and Benomar, L. and Berdugo-Lattke, M. L. and Berenguer, E. and Bergamin, R. and Bergmann, J. and Bergmann Carlucci, M. and Berner, L. and Bernhardt-Römermann, M. and Bigler, C. and Bjorkman, A. D. and Blackman, C. and Blanco, C. and Blonder, B. and Blumenthal, D. and Bocanegra-González, K. T. and Boeckx, P. and Bohlman, S. and Böhning-Gaese, K. and Boisvert-Marsh, L. and Bond, W. and Bond-Lamberty, B. and Boom, A. and Boonman, C. C. F. and Bordin, K. and Boughton, E. H. and Boukili, V. and Bowman, D. M. J. S. and Bravo, S. and Brendel, M. R. and Broadley, M. R. and Brown, K. A. and Bruelheide, H. and Brumnich, F. and Bruun, H. H. and Bruy, D. and Buchanan, S. W. and Bucher, S. F. and Buchmann, N. and Buitenwerf, R. and Bunker, D. E. and Bürger, J. and Burrascano, S. and Burslem, D. F. R. P. and Butterfield, B. J. and Byun, C. and Marques, M. and Scalon, M. C. and Caccianiga, M. and Cadotte, M. and Cailleret, M. and Camac, J. and Camarero, J. J. and Campany, C. and Campetella, G. and Campos, J. A. and Cano-Arboleda, L. and Canullo, R. and Carbognani, M. and Carvalho, F. and Casanoves, F. and Castagneyrol, B. and Catford, J. A. and Cavender-Bares, J. and Cerabolini, B. E. L. and Cervellini, M. and Chacón-Madrigal, E. and Chapin, K. and Chapin, F. S. and Chelli, S. and Chen, S.-C. and Chen, A. and Cherubini, P. and Chianucci, F. and Choat, B. and Chung, K.-S. and Chytrý, M. and Ciccarelli, D. and Coll, L. and Collins, C. G. and Conti, L. and Coomes, D. and Cornelissen, J. H. C. and Cornwell, W. K. and Corona, P. and Coyea, M. and Craine, J. and Craven, D. and Cromsigt, J. P. G. M. and Csecserits, A. and Cufar, K. and Cuntz, M. and da Silva, A. C. and Dahlin, K. M. and Dainese, M. and Dalke, I. and Dalle Fratte, M. and Dang-Le, A. T. and Danihelka, J. and Dannoura, M. and Dawson, S. and de Beer, A. J. and De Frutos, A. and De Long, J. R. and Dechant, B. and Delagrange, S. and Delpierre, N. and Derroire, G. and Dias, A. S. and Diaz-Toribio, M.

https://doi.org/10.5194/egusphere-2025-318
Preprint. Discussion started: 24 January 2025

H. and Dimitrakopoulos, P. G. and Dobrowolski, M. and Doktor, D. and Dřevojan, P. and Dong, N. and Dransfield, J. and Dressler, S. and Duarte, L. and Ducouret, E. and Dullinger, S. and Durka, W. and Duursma, R. and Dymova, O. and E-Vojtkó, A. and Eckstein, R. L. and Ejtehadi, H. and Elser, J. and Emilio, T. and Engemann, K. and Erfanian, M. B. and Erfmeier, A. and Esquivel-Muelbert, A. and Esser, G. and Estiarte, M. and Domingues, T. F. and Fagan, W. F. and Fagúndez, J. and Falster, D. S. and Fan, Y. and Fang, J. and Farris, E. and Fazlioglu, F. and Feng, Y. and Fernandez-Mendez, F. and Ferrara, C. and Ferreira, J. and Fidelis, A. and Finegan, B. and Firn, J. and Flowers, T. J. and Flynn, D. F. B. and Fontana, V. and Forey, E. and Forgiarini, C. and François, L. and Frangipani, M. and Frank, D. and Frenette-Dussault, C. and Freschet, G. T. and Fry, E. L. and Fyllas, N. M. and Mazzochini, G. G. and Gachet, S. and Gallagher, R. and Ganade, G. and Ganga, F. and García-Palacios, P. and Gargaglione, V. and Garnier, E. and Garrido, J. L. and de Gasper, A. L. and Gea-Izquierdo, G. and Gibson, D. and Gillison, A. N. and Giroldo, A. and Glasenhardt, M.-C. and Gleason, S. and Gliesch, M. and Goldberg, E. and Göldel, B. and Gonzalez-Akre, E. and Gonzalez-Andujar, J. L. and González-Melo, A. and González-Robles, A. and Graae, B. J. and Granda, E. and Graves, S. and Green, W. A. and Gregor, T. and Gross, N. and Guerin, G. R. and Günther, A. and Gutiérrez, A. G. and Haddock, L. and Haines, A. and Hall, J. and Hambuckers, A. and Han, W. and Harrison, S. P. and Hattingh, W. and Hawes, J. E. and He, T. and He, P. and Heberling, J. M. and Helm, A. and Hempel, S. and Hentschel, J. and Hérault, B. and Hereş, A.-M. and Herz, K. and Heuertz, M. and Hickler, T. and Hietz, P. and Higuchi, P. and Hipp, A. L. and Hirons, A. and Hock, M. and Hogan, J. A. and Holl, K. and Honnay, O. and Hornstein, D. and Hou, E. and Hough-Snee, N. and Hovstad, K. A. and Ichie, T. and Igić, B. and Illa, E. and Isaac, M. and Ishihara, M. and Ivanov, L. and Ivanova, L. and Iversen, C. M. and Izquierdo, J. and Jackson, R. B. and Jackson, B. and Jactel, H. and Jagodzinski, A. M. and Jandt, U. and Jansen, S. and Jenkins, T. and Jentsch, A. and Jespersen, J. R. P. and Jiang, G.-F. and Johansen, J. L. and Johnson, D. and Jokela, E. J. and Joly, C. A. and Jordan, G. J. and Joseph, G. S. and Junaedi, D. and Junker, R. R. and Justes, E. and Kabzems, R. and Kane, J. and Kaplan, Z. and Kattenborn, T. and Kavelenova, L. and Kearsley, E. and Kempel, A. and Kenzo, T. and Kerkhoff, A. and Khalil, M. I. and Kinlock, N. L. and Kissling, W. D. and Kitajima, K. and Kitzberger, T. and Kjøller, R. and Klein, T. and Kleyer, M. and Klimešová, J. and Klipel, J. and Kloeppel, B. and Klotz, S. and Knops, J. M. H. and Kohyama, T. and Koike, F. and Kollmann, J. and Komac, B. and Komatsu, K. and König, C. and Kraft, N. J. B. and Kramer, K. and Kreft, H. and Kühn, I. and Kumarathunge, D. and Kuppler, J. and Kurokawa, H. and Kurosawa, Y. and Kuyah, S. and Laclau, J.-P. and Lafleur, B. and Lallai, E. and Lamb, E. and Lamprecht, A. and Larkin, D. J. and Laughlin, D. and Le Bagousse-Pinguet, Y. and le Maire, G. and le Roux, P. C. and le Roux, E. and Lee, T. and Lens, F. and Lewis, S. L. and Lhotsky, B. and Li, Y. and Li, X. and Lichstein, J. W. and Liebergesell, M. and Lim, J. Y. and Lin, Y.-S. and Linares, J. C. and Liu, C. and Liu, D. and Liu, U. and Livingstone, S. and Llusià, J. and Lohbeck, M. and López-García, Á. and Lopez-Gonzalez, G. and Lososová, Z. and Louault, F. and Lukács, B. A. and Lukeš, P. and Luo, Y. and Lussu, M. and Ma, S. and Maciel Rabelo Pereira, C. and Mack, M. and Maire, V. and Mäkelä, A. and Mäkinen, H. and Malhado, A. C. M. and Mallik, A. and Manning, P. and Manzoni, S. and Marchetti, Z. and Marchino, L. and Marcilio-Silva, V. and Marcon, E. and Marignani, M. and Markesteijn, L. and Martin, A. and Martínez-Garza, C. and Martínez-Vilalta, J. and Mašková, T. and Mason, K. and Mason, N. and Massad, T. J. and Masse, J. and Mayrose, I. and McCarthy, J. and McCormack, M. L. and McCulloh, K. and McFadden, I. R. and McGill, B. J. and McPartland, M. Y. and Medeiros, J. S. and Medlyn, B. and Meerts, P. and Mehrabi, Z. and Meir, P. and Melo, F. P. L. and Mencuccini, M. and Meredieu, C. and Messier, J. and Mészáros, I. and Metsaranta, J. and Michaletz, S. T. and Michelaki, C. and Migalina, S. and Milla, R. and Miller, J. E. D. and Minden, V. and Ming, R. and Mokany, K. and Moles, A. T. and Molnár V, A. and Molofsky, J. and Molz, M. and Montgomery, R. A. and Monty, A. and Moravcová, L. and Moreno-Martínez, A. and Moretti, M. and Mori, A. S. and Mori, S. and Morris, D. and Morrison, J. and Mucina, L. and Mueller, S. and Muir, C. D. and Müller, S. C. and Munoz, F. and Myers-Smith, I. H. and Myster, R. W. and Nagano, M. and Naidu, S. and Narayanan, A. and Natesan, B. and Negoita, L. and Nelson, A. S. and Neuschulz, E. L. and Ni, J. and Niedrist, G. and Nieto, J. and Niinemets, Ü. and Nolan, R. and Nottebrock, H. and Nouvellon, Y. and Novakovskiy, A. and The Nutrient, N. and Nystuen, K. O. and O'Grady, A. and O'Hara, K. and O'Reilly-Nugent, A. and Oakley, S. and Oberhuber, W. and Ohtsuka, T. and Oliveira, R. and Öllerer, K. and Olson, M. E. and Onipchenko, V. and Onoda, Y. and Onstein, R. E. and Ordonez, J. C. and Osada, N. and Ostonen, I. and Ottaviani, G. and Otto, S. and Overbeck, G. E. and Ozinga, W. A. and Pahl, A. T. and Paine, C. E. T. and Pakeman, R. J. and Papageorgiou, A. C. and Parfionova, E. and Pärtel, M. and Patacca, M. and Paula, S. and Paule, J. and Pauli, H. and Pausas, J. G. and Peco, B. and Penuelas, J. and Perea, A. and Peri, P. L. and Petisco-Souza, A. C. and Petraglia, A. and Petritan, A. M. and Phillips, O. L. and Pierce, S. and Pillar, V. D. and Pisek, J. and Pomogaybin, A. and Poorter, H. and Portsmuth, A. and Poschlod, P. and Potvin, C. and Pounds, D. and Powell, A. S. and Power, S. A. and

https://doi.org/10.5194/egusphere-2025-318
Preprint. Discussion started: 24 January 2025

Prinzing, A. and Puglielli, G. and Pyšek, P. and Raevel, V. and Rammig, A. and Ransijn, J. and Ray, C. A. and Reich, P. B. and Reichstein, M. and Reid, D. E. B. and Réjou-Méchain, M. and de Dios, V. R. and Ribeiro, S. and Richardson, S. and Riibak, K. and Rillig, M. C. and Riviera, F. and Robert, E. M. R. and Roberts, S. and Robroek, B. and Roddy, A. and Rodrigues, A. V. and Rogers, A. and Rollinson, E. and Rolo, V. and Römermann, C. and Ronzhina, D. and Roscher, C. and Rosell, J. A. and Rosenfield, M. F. and Rossi, C. and Roy, D. B. and Royer-Tardif, S. and Rüger, N. and Ruiz-Peinado, R. and Rumpf, S. B. and Rusch, G. M. and Ryo, M. and Sack, L. and Saldaña, A. and Salgado-Negret, B. and Salguero-Gomez, R. and Santa-Regina, I. and Santacruz-García, A. C. and Santos, J. and Sardans, J. and Schamp, B. and Scherer-Lorenzen, M. and Schleuning, M. and Schmid, B. and Schmidt, M. and Schmitt, S. and Schneider, J. V. and Schowanek, S. D. and Schrader, J. and Schrodt, F. and Schuldt, B. and Schurr, F. and Selaya Garvizu, G. and Semchenko, M. and Seymour, C. and Sfair, J. C. and Sharpe, J. M. and Sheppard, C. S. and Sheremetiev, S. and Shiodera, S. and Shipley, B. and Shovon, T. A. and Siebenkäs, A. and Sierra, C. and Silva, V. and Silva, M. and Sitzia, T. and Sjöman, H. and Slot, M. and Smith, N. G. and Sodhi, D. and Soltis, P. and Soltis, D. and Somers, B. and Sonnier, G. and Sørensen, M. V. and Sosinski Jr, E. E. and Soudzilovskaia, N. A. and Souza, A. F. and Spasojevic, M. and Sperandii, M. G. and Stan, A. B. and Stegen, J. and Steinbauer, K. and Stephan, J. G. and Sterck, F. and Stojanovic, D. B. and Strydom, T. and Suarez, M. L. and Svenning, J.-C. and Svitková, I. and Svitok, M. and Svoboda, M. and Swaine, E. and Swenson, N. and Tabarelli, M. and Takagi, K. and Tappeiner, U. and Tarifa, R. and Tauugourdeau, S. and Tavsanoglu, C. and te Beest, M. and Tedersoo, L. and Thiffault, N. and Thom, D. and Thomas, E. and Thompson, K. and Thornton, P. E. and Thuiller, W. and Tichý, L. and Tissue, D. and Tjoelker, M. G. and Tng, D. Y. P. and Tobias, J. and Török, P. and Tarin, T. and Torres-Ruiz, J. M. and Tóthmérész, B. and Treurnicht, M. and Trivellone, V. and Trolliet, F. and Trotsiuk, V. and Tsakalos, J. L. and Tsiripidis, I. and Tysklind, N. and Umehara, T. and Usoltsev, V. and Vadeboncoeur, M. and Vaezi, J. and Valladares, F. and Vamosi, J. and van Bodegom, P. M. and van Breugel, M. and Van Cleemput, E. and van de Weg, M. and van der Merwe, S. and van der Plas, F. and van der Sande, M. T. and van Kleunen, M. and Van Meerbeek, K. and Vanderwel, M. and Vanselow, K. A. and Vårhammar, A. and Varone, L. and Vasquez Valderrama, M. Y. and Vassilev, K. and Vellend, M. and Veneklaas, E. J. and Verbeeck, H. and Verheyen, K. and Vibrans, A. and Vieira, I. and Villacís, J. and Violle, C. and Vivek, P. and Wagner, K. and Waldram, M. and Waldron, A. and Walker, A. P. and Waller, M. and Walther, G. and Wang, H. and Wang, F. and Wang, W. and Watkins, H. and Watkins, J. and Weber, U. and Weedon, J. T. and Wei, L. and Weigelt, P. and Weiher, E. and Wells, A. W. and Wellstein, C. and Wenk, E. and Westoby, M. and Westwood, A. and White, P. J. and Whitten, M. and Williams, M. and Winkler, D. E. and Winter, K. and Womack, C. and Wright, I. J. and Wright, S. J. and Wright, J. and Pinho, B. X. and Ximenes, F. and Yamada, T. and Yamaji, K. and Yanai, R. and Yankov, N. and Yguel, B. and Zanini, K. J. and Zanne, A. E. and Zelený, D. and Zhao, Y.-P. and Zheng, J. and Zheng, J. and Ziemińska, K. and Zirbel, C. R. and Zizka, G. and Zo-Bi, I. C. and Zotz, G. and Wirth, C.: TRY plant trait database – enhanced coverage and open access, Global Change Biology, 26, 119-188, 10.1111/gcb.14904, 2020.

Knapp, N., Fischer, R., and Huth, A.: Linking lidar and forest modeling to assess biomass estimation across scales and disturbance states, Remote Sensing of Environment, 205, 199-209, https://doi.org/10.1016/j.rse.2017.11.018, 2018.

Laliberté, E., Schweiger, A. K., and Legendre, P.: Partitioning plant spectral diversity into alpha and beta components, Ecology Letters, 23, 370-380, 10.1111/ele.13429, 2020.

Lam, S. K., Pitrou, A., and Seibert, S.: Numba: A llvm-based python jit compiler, Proceedings of the Second Workshop on the LLVM Compiler Infrastructure in HPC, 1-6,

Leuning, R., Zhang, Y. Q., Rajaud, A., Cleugh, H., and Tu, K.: A simple surface conductance model to estimate regional evaporation using MODIS leaf area index and the Penman-Monteith equation, Water Resources Research, 44, https://doi.org/10.1029/2007WR006562, 2008.

Li, W., Pacheco-Labrador, J., Migliavacca, M., Miralles, D., Hoek van Dijke, A., Reichstein, M., Forkel, M., Zhang, W., Frankenberg, C., Panwar, A., Zhang, Q., Weber, U., Gentine, P., and Orth, R.: Widespread and complex drought effects on vegetation physiology inferred from space, Nature Communications, 14, 4640, 10.1038/s41467-023-40226-9, 2023.

Ludwig, A., Doktor, D., and Feilhauer, H.: Is spectral pixel-to-pixel variation a reliable indicator of grassland biodiversity? A systematic assessment of the spectral variation hypothesis using spatial simulation experiments, Remote Sensing of Environment, 302, 113988, https://doi.org/10.1016/j.rse.2023.113988, 2024.

Luo, X., Croft, H., Chen, J. M., He, L., and Keenan, T. F.: Improved estimates of global terrestrial photosynthesis using information on leaf chlorophyll content, Global Change Biology, 25, 2499-2514, 10.1111/gcb.14624, 2019.

https://doi.org/10.5194/egusphere-2025-318
Preprint. Discussion started: 24 January 2025

Ma, X., Mahecha, M. D., Migliavacca, M., van der Plas, F., Benavides, R., Ratcliffe, S., Kattge, J., Richter, R., Musavi, T., Baeten, L., Barnoaiea, I., Bohn, F. J., Bouriaud, O., Bussotti, F., Coppi, A., Domisch, T., Huth, A., Jaroszewicz, B., Joswig, J., Pabon-Moreno, D. E., Papale, D., Selvi, F., Laurin, G. V., Valladares, F., Reichstein, M., and Wirth, C.: Inferring plant functional diversity from space: the potential of Sentinel-2, Remote Sensing of Environment, 233, 111368, https://doi.org/10.1016/j.rse.2019.111368, 2019.

Mahecha, M. D., Bastos, A., Bohn, F., Eisenhauer, N., Feilhauer, H., Hickler, T., Kalesse-Los, H., Migliavacca, M., Otto, F. E. L., Peng, J., Tegen, I., Weigelt, A., Wendisch, M., Wirth, C., Al-Halbouni, D., Deneke, H. M., Doktor, D., Dunker, S., Ehrlich, A., Foth, A., García-García, A., Guerra, C. A., Guimarães-Steinicke, C., Hartmann, H., Henning, S., Herrmann, H., Ji, C., Kattenborn, T., Kolleck, N., Kretschmer, M., Kühn, I., Luttkus, M. L., Maahn, M., Mönks, M., Mora, K., Pöhlker, M., Reichstein, M., Rüger, N., Sánchez-Parra, B., Schäfer, M., Sippel, S., Tesche, M., Wehner, B., Wieneke, S., Winkler, A., Wolf, S., Zaehle, S., Zscheischler, J., and Quaas, J.: Biodiversity and climate extremes: known interactions and research gaps, ESS Open Archive, 10.22541/essoar.169462031.19744802/v1, 2023.

Migliavacca, M., Reichstein, M., Richardson, A. D., Colombo, R., Sutton, M. A., Lasslop, G., Tomelleri, E., Wohlfahrt, G., Carvalhais, N., Cescatti, A., Mahecha, M. D., Montagnani, L., Papale, D., Zaehle, S., Arain, A., Arneth, A., Black, T. A., Carrara, A., Dore, S., Gianelle, D., Helfter, C., Hollinger, D., Kutsch, W. L., Lafleur, P. M., Nouvellon, Y., Rebmann, C., Da Rocha, H. R., Rodeghiero, M., Roupsard, O., SebastiÀ, M.-T., Seufert, G., Soussana, J.-F., and Van Der Molen, M. K.: Semiempirical modeling of abiotic and biotic factors controlling ecosystem respiration across eddy covariance sites, Global Change Biology, 17, 390-409, https://doi.org/10.1111/j.1365-2486.2010.02243.x, 2011.

Miner, G., L., Bauerle, W., L., and Baldocchi, D., D.: Estimating the sensitivity of stomatal conductance to photosynthesis: a review, Plant, Cell & Environment, 40, 1214-1238, 10.1111/pce.12871, 2016.

Monteith, J. L.: Evaporation and environment, Symp Soc Exp Biol, 19, 205-234, 1965.

Oh, Y. and Kweon, S. G.: A simple and accurate model for radar backscattering from vegetation-covered surfaces, 2013 Proceedings of the International Symposium on Antennas & Propagation, 23-25 Oct. 2013, 1179-1182,

Pacheco-Labrador, J., de Bello, F., Migliavacca, M., Ma, X., Carvalhais, N., and Wirth, C.: A generalizable normalization for assessing plant functional diversity metrics across scales from remote sensing, Methods in Ecology and Evolution, 14, 2123-2136, https://doi.org/10.1111/2041-210X.14163, 2023.

Pacheco-Labrador, J., Migliavacca, M., Ma, X., Mahecha, M. D., Carvalhais, N., Weber, U., Benavides, R., Bouriaud, O., Barnoaiea, I., Coomes, D. A., Bohn, F. J., Kraemer, G., Heiden, U., Huth, A., and Wirth, C.: Challenging the link between functional and spectral diversity with radiative transfer modeling and data, Remote Sensing of Environment, 280, 113170, https://doi.org/10.1016/j.rse.2022.113170, 2022.

Pacheco-Labrador, J., Cendrero-Mateo, M. P., Van Wittenberghe, S., Hernandez-Sequeira, I., Koren, G., Prikaziuk, E., Fóti, S., Tomelleri, E., Maseyk, K., Čereković, N., Gonzalez-Cascon, R., Malenovský, Z., Albert-Saiz, M., Antala, M., Balogh, J., Buddenbaum, H., Dehghan-Shoar, M. H., Fennell, J. T., Féret, J.-B., Balde, H., Machwitz, M., Mészáros, Á., Miao, G., Morata, M., Naethe, P., Nagy, Z., Pintér, K., Pullanagari, R. R., Rastogi, A., Siegmann, B., Wang, S., Zhang, C., and Kopkáně, D.: Ecophysiological variables retrieval and early stress detection: insights from a synthetic spatial scaling exercise, International Journal of Remote Sensing, 1-26, 10.1080/01431161.2024.2414435, 2024.

Palmer, M. W., Wohlgemuth, T., Earls, P., Arévalo, J., and Thompson, S.: Opportunities for long-term ecological research at the Tallgrass Prairie Preserve, Oklahoma, Proceedings of the ILTER regional workshop: cooperation in long term ecological research in Central and Eastern Europe, Budapest, Hungary,

Pereira, H. M., Ferrier, S., Walters, M., Geller, G. N., Jongman, R. H. G., Scholes, R. J., Bruford, M. W., Brummitt, N., Butchart, S. H. M., Cardoso, A. C., Coops, N. C., Dulloo, E., Faith, D. P., Freyhof, J., Gregory, R. D., Heip, C., Höft, R., Hurtt, G., Jetz, W., Karp, D. S., McGeoch, M. A., Obura, D., Onoda, Y., Pettorelli, N., Reyers, B., Sayre, R., Scharlemann, J. P. W., Stuart, S. N., Turak, E., Walpole, M., and Wegmann, M.: Essential Biodiversity Variables, Science, 339, 277, 10.1126/science.1229931, 2013.

Rocchini, D., Thouverai, E., Marcantonio, M., Iannacito, M., Da Re, D., Torresani, M., Bacaro, G., Bazzichetto, M., Bernardi, A., Foody, G. M., Furrer, R., Kleijn, D., Larsen, S., Lenoir, J., Malavasi, M., Marchetto, E., Messori, F., Montaghi, A., Moudrý, V., Naimi, B., Ricotta, C., Rossini, M., Santi, F., Santos, M. J., Schaepman, M. E., Schneider, F. D., Schuh, L., Silvestri, S., Šímová, P., Skidmore, A. K., Tattoni, C., Tordoni, E., Vicario, S., Zannini, P., and Wegmann, M.: rasterdiv—An Information Theory tailored R package for measuring ecosystem heterogeneity from space: To the origin and back, Methods in Ecology and Evolution, 12, 1093-1102, https://doi.org/10.1111/2041-210X.13583, 2021.

https://doi.org/10.5194/egusphere-2025-318
Preprint. Discussion started: 24 January 2025

Rossi, C. and Gholizadeh, H.: Uncovering the hidden: Leveraging sub-pixel spectral diversity to estimate plant diversity from space, Remote Sensing of Environment, 296, 113734, https://doi.org/10.1016/j.rse.2023.113734, 2023.

Rossi, C., Kneubühler, M., Schütz, M., Schaepman, M. E., Haller, R. M., and Risch, A. C.: Remote sensing of spectral diversity: A new methodological approach to account for spatio-temporal dissimilarities between plant communities, Ecological Indicators, 130, 108106, https://doi.org/10.1016/j.ecolind.2021.108106, 2021.

Rouse, J. W., Haas, R. H., Schell, J. A., and Deering, D. W.: Monitoring vegetation systems in the Great Plains with ERTS, Third Earth Resources Technology Satellite- 1 Symposium, Greenbelt, MD, USA, 301–317,

Rubel, F., Brugger, K., Haslinger, K., and Auer, I.: The climate of the European Alps: Shift of very high resolution Köppen-Geiger climate zones 1800–2100, Meteorologische Zeitschrift, 26, 115-125, 10.1127/metz/2016/0816, 2017.

Schweiger, A. K., Cavender-Bares, J., Townsend, P. A., Hobbie, S. E., Madritch, M. D., Wang, R., Tilman, D., and Gamon, J. A.: Plant spectral diversity integrates functional and phylogenetic components of biodiversity and predicts ecosystem function, Nature Ecology & Evolution, 2, 976-982, 10.1038/s41559-018-0551-1, 2018.

Tagliabue, G., Panigada, C., Celesti, M., Cogliati, S., Colombo, R., Migliavacca, M., Rascher, U., Rocchini, D., Schüttemeyer, D., and Rossini, M.: Sun–induced fluorescence heterogeneity as a measure of functional diversity, Remote Sensing of Environment, 247, 111934, https://doi.org/10.1016/j.rse.2020.111934, 2020.

Torresani, M., Rossi, C., Perrone, M., Hauser, L. T., Féret, J.-B., Moudrý, V., Simova, P., Ricotta, C., Foody, G. M., Kacic, P., Feilhauer, H., Malavasi, M., Tognetti, R., and Rocchini, D.: Reviewing the spectral variation hypothesis: Twenty years in the tumultuous sea of biodiversity estimation by remote sensing, Ecological Informatics, 102702, https://doi.org/10.1016/j.ecoinf.2024.102702, 2024.

Van Cleemput, E., Adler, P., and Suding, K. N.: Making remote sense of biodiversity: What grassland characteristics make spectral diversity a good proxy for taxonomic diversity?, Global Ecology and Biogeography, 32, 2177-2188, https://doi.org/10.1111/geb.13759, 2023.

van der Tol, C., Verhoef, W., Timmermans, J., Verhoef, A., and Su, Z.: An integrated model of soil-canopy spectral radiances, photosynthesis, fluorescence, temperature and energy balance, Biogeosciences, 6, 3109-3129, 10.5194/bg-6-3109-2009, 2009.

van Leeuwen, M., Frye, H. A., and Wilson, A. M.: Understanding limits of species identification using simulated imaging spectroscopy, Remote Sensing of Environment, 259, 112405, https://doi.org/10.1016/j.rse.2021.112405, 2021.

Vremec, M., Collenteur, R. A., and Birk, S.: Technical note: Improved handling of potential evapotranspiration in hydrological studies with PyEt, Hydrol. Earth Syst. Sci. Discuss., 2023, 1-23, 10.5194/hess-2022-417, 2023.

Wallace and Verhoef, A.: Modelling interactions in mixed-plant communities: light, water and carbon dioxide. In: Leaf development and canopy growth, in: Leaf development and canopy growth, edited by: Marshall B., R. J. A., Sheffield biological science series, Sheffield Academic Press, Sheffield, 204–250, 2000.

Wang, Q., Tang, Y., and Atkinson, P. M.: The effect of the point spread function on downscaling continua, ISPRS Journal of Photogrammetry and Remote Sensing, 168, 251-267, https://doi.org/10.1016/j.isprsjprs.2020.08.016, 2020.

Wang, R., Gamon, J. A., Cavender-Bares, J., Townsend, P. A., and Zygielbaum, A. I.: The spatial sensitivity of the spectral diversity–biodiversity relationship: an experimental test in a prairie grassland, Ecological Applications, 28, 541-556, 10.1002/eap.1669, 2018.

Yang, P., Prikaziuk, E., Verhoef, W., and van der Tol, C.: SCOPE 2.0: a model to simulate vegetated land surface fluxes and satellite signals, Geosci. Model Dev., 14, 4697-4712, 10.5194/gmd-14-4697-2021, 2021.

Zhao, Y., Zeng, Y., Zheng, Z., Dong, W., Zhao, D., Wu, B., and Zhao, Q.: Forest species diversity mapping using airborne LiDAR and hyperspectral data in a subtropical forest in China, Remote Sensing of Environment, 213, 104-114, https://doi.org/10.1016/j.rse.2018.05.014, 2018.